Tunnelling and Underground Space Technology 146 (2024) 105637

Contents lists available at ScienceDirect

Tunnelling and Underground Space Technology

journal homepage: www.elsevier.com/locate/tust

Optimizing fire emergency evacuation routes in underground coal mines: A lightweight network flow approach

Simon Lotero [a], Vasilis Androulakis [a,*], Hassan Khaniani [b], Mostafa Hassanalian [c], Sihua Shao [d], Pedram Roghanchi [e]

[a] Department of Mineral Engineering, New Mexico Tech, Socorro, NM 87801, USA
[b] Petroleum Recovery Research Center, New Mexico Tech, Socorro, NM 87801, USA
[c] Department of Mechanical Engineering, New Mexico Tech, Socorro, NM 87801, USA
[d] Department of Electrical Engineering, New Mexico Tech, Socorro, NM 87801, USA
[e] Department of Mining Engineering, University of Kentucky, Lexington, KY 46504, USA

ARTICLE INFO

Keywords:
Ford-Fulkerson algorithm
Mine fire emergency
Mine ventilation simulation
Self-evacuation

ABSTRACT

In underground mine fires, the presence of smoke, toxic gasses, and high heat can significantly hinder the evacuees from identifying the optimal path to safety. This study presents a framework that couples a mine fire simulator software with a Ford-Fulkerson algorithm to model fire evacuations as a minimum-cost flow problem. The fire-induced risks are quantified based on the MSHA safety standards and a user-friendly FFA computes the evacuation routes. By accumulating the quantified effect of the risk exposure and updating the network depending on the mine conditions, different safe evacuation routes are identified. The algorithm is demonstrated through fire simulation data acquired from a model of the VentSim™ DESIGN software. Airflow quantity, air quality, heat, carbon monoxide concentration, and visibility obstruction are acquired from the simulations and processed through the proposed algorithm. Based on the distribution of the quantified hazards and the MSHA safety standards, the algorithm outputs optimal evacuation paths. The computed evacuation routes minimize the exposure to the fire-induced hazards while at the same time prioritize the shortest routes. The presented framework can be used for evaluating ventilation designs and emergency plans as well as in real-time self-evacuation in mine emergencies.

1. Introduction

Historically, underground mining has been one of the most hazardous occupations due to the dynamic and harsh occupational conditions, such as high heat, darkness, dust, heavy machinery, confined spaces, and the lack of fresh air. Some of the hazards miners face daily are explosions, fires, floods, and roof falls that expose their lives and health to danger. One of the most dangerous, dynamic emergencies in underground coal mines is the occurrence of fires. Fire is the second most frequent cause of death throughout the history of mining in the USA with 35 incidents claiming 727 lives in the period between 1900–2008. Furthermore, in the same period, the most frequent accidents in underground coal mines were explosions, which often ignite fires (Brnich et al., 2010; Kowalski-Trakofler et al., 2009). Additionally, fires damage the mine infrastructure and cause large economic losses to the mining industry. Despite the decline in fire incidents due to the improvement of safety practices, as well as the implementation of recent technologies towards preventative or mitigating measures, fires remain a constant concern in the mining industry (Goh, 2021; Mahdevari et al., 2014; Ray and Singh, 2007; Yang et al., 2022a).

Several factors such as the amount of flammable material, the place of ignition, the layout of the ventilation system, and the time at which the fire breaks out, make it difficult to predict hazard locations inside the mine and execute an optimal evacuation plan. Mine fires can lead to explosions of flammable materials in the mine, produce excessive smoke and irritant gasses that restrict visibility, disorient the miners, and impede self-escape, while at the same time can significantly damage the mine infrastructure and delay production (Düzgün and Leveson, 2018; Brake, 2013).

In their study of underground coal mine disaster in the USA for 1900–2010, Brnich et al. (2010) identified six major disasters, out of which one was a fire and claimed the lives of two miners. Although, the most frequent accidents in USA underground coal mines for the same period are explosions, the explosions can often ignite fires. Explosions can have a great impact in claiming lives and causing damages in

* Corresponding author.
E-mail address: vasileios.androulakis@nmt.edu (V. Androulakis).

https://doi.org/10.1016/j.tust.2024.105637
Received 18 May 2023; Received in revised form 19 January 2024; Accepted 31 January 2024
Available online 9 February 2024

the vicinity of their occurrence, but fires can spread rapidly through entries with propagation rates more than 0.10 m/s (Conti, 2001). Mine Safety and Health Administration (MSHA) accident reports between 1991 and 2000 indicate that 137 fires, independently of size or fatalities, have been reported in underground coal, metal and non-metal mines (Conti et al., 2005). The study of Conti et al. (2005) identifies six main categories of mine fires in coal and metal/nonmetal underground mines: (a) electrical, (b) friction, (c) mobile equipment, (d) spontaneous combustion, (e) cutting/welding, and (f) other. The same study finds that "friction is the most common cause of underground coal mine fires, while mobile equipment malfunction is the leading cause of fires in underground metal/nonmetal mines". Between 2001 and 2010, ten miners died of gas poisoning due to prolonged entrapment caused by insufficient evacuation measures in the mine. Although there were no fatalities directly caused by fires after 2000, this phenomenon is still recurrent and is a potential danger for miners.

Effective and timely escape from contaminated environments prevents irreversible health effects or even death. Escape practices in mine emergencies are dictated through a series of protocols and procedures that allows a mine to respond, establish control, and escape from danger quickly. All mine personnel must attend training to the mine evacuation protocols. Mine preparedness is constantly dependent on factors such as knowledge of the dynamic environment, the ability to respond to hazards, and the establishment of effective communication for decision-making. In emergencies, miner decision-making determines the success of survival and controls the evacuation flow. Miner decision-making in underground mines refers to how miners choose desirable alternatives to self-evacuate in the event of an emergency. Naturally, the evacuation flow and the gasses flow overlap during the response period because they are sharing the same spatial network of the mine openings. Therefore, identifying the pathways with the highest risk is of vital importance to the optimization of the escape paths that minimize exposure to these risks for the miners (Adjiski et al., 2015; Onifade, 2021; Conti et al., 2005; Ryan and Watkinson, 2017).

A variety of ventilation simulation software that provide evacuation optimization tools are available to the mining industry. Despite these simulators providing critical insights regarding ventilation and emergency evacuation practices, further analysis of the simulation data is often necessary to acquire the desired output. Flow network modeling is a commonly tool used to optimize emergency evacuation routes in a variety of environments such as cruise ships, urban underground tunnels, buildings, or cities (Chalmet et al., 1982; Liu et al., 2022; Deng et al., 2022; Hamacher and Tjandra, 2001; Yang et al., 2022b).

The current study identifies a gap in mine emergency measures and decision-making practices regarding the flexibility of integrating the current safety standards as well as the dynamic state of a mine ventilation system into emergency evacuation planning and real-time decision-making. Therefore, this study presents a lightweight and user-friendly approach that couples data extracted from a mine fire simulation software with a Ford–Fulkerson algorithm (FFA) to model a flow network and optimize evacuation routes considering the dynamic propagation of fire-induced risks inside the mine.

The rest of the paper is structured as follows: Section 2 provides background about fire simulation tools, and flow network algorithms used for evacuation planning. In Section 3 the fire simulation conducted and the custom FFA used for solving the evacuation problem are presented, while Section 4 presents the results of the fire simulation and the FFA evacuation path planning. Finally, Section 5 presents the conclusions and discusses the main takeaways from this study.

2. Fire emergencies in underground mines

In recent decades, extensive research on underground fire disasters has been conducted with an emphasis on decision-making optimization in a mine fire evacuation. Rescue preparedness, recovery, miner response, and evacuation training have been the main points of study. However, the many unknown parameters in a dynamic fire disaster impose limitations on timely decision-making. The location of the fire, the flow of the hazardous gases, and the mental stress of the trapped miners are unknowns that affect the planning of the safest escape measures. Preparedness is an essential element of any underground mine's strategic plan in dealing with an emergency evacuation. Time is a critical factor, and any delay may mean severe injury or death. Therefore, it is important that the fire be detected in the incipient stage and that well-trained and equipped miners respond during that crucial period. A crucial element to consider in any fire safety program is adequate firsthand training for the entire workforce.

A critical component in a mine fire evacuation is the ventilation system of a mine. The design of a ventilation system of an underground mine aim to prevent and control fire emergencies, as well as direct the flow of gases out of the mine. The gasses created by the fire are a dynamic problem due to their constant displacement through the mine openings by the ventilation system (Sasmito et al., 2013; Roy et al., 2022; Conti et al., 2005). Since the dynamics of a fire and the mine ventilation design are closely related, mine ventilation design software usually provides fire simulation tools. Commonly used software include: MFIRE 4.0 (Zhou and Schall, 2020), VUMA3D-network (Vuma Software, 2023), PyroSim (Thunderhead Engineering, 2023), VentGraph (IMG PAN, 2023), MineFire (SRK Consulting (Global) Lmt., 2023), and VentSim™ DESIGN (Howden Group, 2020). A mine ventilation system is a complex and dynamic system that is dependent on various components, such as the entry/crosscuts geometry, ventilation fans, ventilation curtains, overcast ducts, etc. In a mine emergency, the state and performance of these components can drastically change, resulting to similarly drastic alterations to the airflow and consequently the propagation of the emergency-induces hazards within the mine. The performance of the ventilation fans can drop or even eliminated, the ventilation curtains can be destroyed, roof failures can change the geometry of the airways or the overcast air-ducts. Although such phenomena can rapidly change the airflow quantity and directions, hence affect the safety of a pathway, they cannot be fully modeled with the existing software.

Evacuation problems are commonly modeled and studied through network flow models. A plethora of algorithms that solve path planning in flow networks have been developed over the years. Traditional algorithms include Dijkstra and A* algorithms, particle swarm optimization, genetic algorithms, cellular automata, ant colony optimization, hybrid approaches, and other intelligent algorithms (Liu et al., 2021; Yu et al., 2019). These algorithms can be applied for static or dynamic models, single- or multi-source to single- or multi-sink problems, as well as single- or multi-objective path planning. The division between maximum flow problems (MFP) and quickest flow problems (QFP) encompasses the majority of these approaches. Flow capacity constraints or maximum flow quantity, minimum travel time, shortest travel distance, minimum travel cost objectives are integrated to allow for path planning optimization (Hamacher and Tjandra, 2001; Liu et al., 2021; Li et al., 2021; Burkard et al., 1993).

Chalmet et al. (1982) developed a maximum-flow minimum-cost (MFMC) approach that simultaneously maximizes the total number of people evacuating a building and minimizes the evacuation time. Lin et al. (2008) presented a multi-stage time-varying quickest flow (MSTVQF) approach to model fire emergency evacuation scheduling in complex buildings and identify bottlenecks. Liu et al. (2022) integrates binary search into a maximum flow algorithm for city evacuation path planning during natural or epidemic disasters. Jin et al. (2021) propose a multi-source, multi-sink MFMC approach for pedestrian evacuation routes to underground shelters. Yang et al. (2022b) use the evolutionary algorithm NSGA-II to formulate a multiobjective evacuation path planning model for multiple fires emergencies in subway stations, while Coutinho-Rodrigues et al. (2012) use Mixed-Integer

Linear Programming Model (MILP) solver for a multiobjective evacuation problem that routes people to multiple shelters in an urban environment. Liu et al. (2021) present an ant colony system that considers crowd density and speed for multipath crowd evacuation from cruise ships. Deng et al. (2022) use Ford-Fulkerson algorithm (FFA) and the shortest path SPFA algorithm to solve a multi-source, multi-sink maximum flow model of a fire emergency on a cruise ship. Simulation data for temperature and toxic gas concentration define the accessibility of an evacuation path.

Despite the variety of environments studied in regard to emergency evacuation planning, a gap is identified when underground mine evacuation is considered. Although, the various ventilation design software assist in emergency planning, there has not been established a robust framework that can integrate real-time data and assist miners to self-evacuate. This study aims to provide the basic concept of such a framework and demonstrate its feasibility. A FFA is implemented to solve a single-source and single-sink minimum cost model of a fire emergency in underground mines. The objective is to minimize the risk along the evacuation route. Ford-Fulkerson algorithm is a lightweight and user-friendly routine that can provide reliable results for this capacity-constraint flow network problem. VentFIRE™ is used to simulate a fire in a room and pillar underground mine. The simulations are used to measure the fire-induced toxic gases, oxygen reduction, heat and visibility obstruction throughout the mine. Subsequently, the simulation data are converted to quantified health risks that are attached to a graph network. Finally, an FFA iterates greedily through all possible paths and eliminates the ones that do not fulfill the corresponding MSHA health and safety standards with the ultimate aim to compute the safest evacuation routes.

3. Simulation and graph network model

In this study, a model of a room and pillar mine with a full ventilation system is used with the VentSim™ DESIGN (version 5.4) software package. Additionally, the configuration of a fire is defined, and a fire simulation is simulated. The goal of the simulation is to obtain the spatiotemporal propagation of the fresh air, the fire fumes, and the heat waves inside the mine. The simulation model includes a room and pillar underground coal mine, a ventilation system, safety measures, a specified sensors layout, and a fire model; the main aspects of these are described below.

3.1. Ventilation system

The ventilation design corresponds to an underground room and pillar coal mine. The ventilation model used is one of the built-in models of the VentSim™ DESIGN package and was modified according to the simulation's purposes (Fig. 1). The simulated mine model used includes two coal panels (hereafter will be distinctively referred to as western and eastern coal panels) that are accessed by a five-entry system. The panels width, beyond the main entry system, extends to both sides for at least one additional entry. The intake air (blue color) is circulating the fresh air through a double entry retreating system. The flow in this ventilation system is directed to the south and the east. The fresh air (blue color) is delivered through the central airways of the mine and the contaminated air is exhausted along the side of the coal panel for the return air (red color). In both panels, the two easternmost panel entries are designated as return air pathways and are isolated from the remaining panel entries with the help of ventilation curtains (see 'stoppings' in Fig. 1). Additionally, the return air pathways of the two panels are connected through overcast air ducts that bypass the fresh air pathways of the eastern coal panel. The return air is extracted by surface-mounted fans positioned in the south of the eastern coal panel and the south-western end of the western panel (green points - booster fans). The ventilation model includes two types of axial fans: the air is exhausted by two Axial Fans 1600/29992 (+30 Deg Bucket Pitch), while six Axial Flow 18.5 kW standard 2 Pole Fans (760 mm) help to propel the air through the intake air (booster fans) and correct the pressure in the model (Yang et al., 2022a; Howden Group, 2020). Although the model has more fans, these are the ones that affect the case study.

The coal is being transported along the longwall face in the same direction as the airflow to reduce the number of contaminants in the mine. The conveyor is installed along the center airway with a brattice curtain regulating the airflow, and a system of stoppings (ventilation seals) to separate the intake air from the return air for both sides of the mine. The traveling road (cyan color) is for the equipment and the personnel, while the belt road (brown color) is for the transportation of the extracted material. The purple area denotes a sealed part of the coal mine, which has been fully extracted and therefore does not affect the ventilation dynamics.

The simulation model assumes an active face (working area) at the northeast side of the eastern coal panel, whereas a refuge chamber is located on the western side of the same coal panel south of the working area. The fire simulation assumes that a fire incident occurs along the main traveling road (cyan color). Although the location of the fire incident has not been deterministically selected, it serves as a location that creates gradual hindrances to the workers escape without fully closing off the principal escape route (which would happen if the ignition location was selected to be on the return airways). The general layout of the simulation model, as well as the layout of the ventilation system dictates that the workers have two options: (a) move northbound (towards the fire) and try to escape through the eastern return air pathways, or (b) move southbound and seek shelter at the refuge chamber. The optimal option will be defined by the time passed between the start of the fire and the time the workers are alerted, as well as the type and burn rate of the fire. These factors determine the progress of the fire and the propagation rate of the fumes in the mine tunnels.

3.2. Sensor simulation

The fire simulation in the ventilation model is executed using VentFIRE™ a subprogram of VentSim™ DESIGN. The VentFIRE™ tool collects data about the spatiotemporal progress of fire-induced heat waves, carbon monoxide, and other fumes. Although the software can simulate and visualize (through colored contours) the different parameters over the ventilation system, the computed values are available for extraction by 'installing' sensors for these parameters at the desired location in the VentSim™ DESIGN model.

To reduce the computational cost, only a segment of the ventilation system is monitored through simulated sensors. The sensors are 'installed' at the area that covers the imminent surroundings of the working area and the fire, as well as the most possible self-evacuation routes (see red-dotted enclosed portion of the model in Fig. 2). The sensors layout 'starts' at the work area and 'moves' north-wise along both the intake air and the return air pathways. Although it would be ideal to install sensors on all the joints of a grid that follows the dimensions of the room-and-pillar model, the number of sensors required would lead to increased complexity and processing time for computing the optimized paths. Therefore, this demonstration of the proposed approach is based on a simplified, non-symmetrical grid of sensors. Although, the simplified sensors mesh leads to a limited number of available evacuation routes compared to reality, it can model sufficiently the dynamic nature of safe evacuation routes over the duration of an emergency event.

Thirty-one (31) sensors were 'installed' with an average horizontal distance of 49.4 m (every three rows of pillars) and an average vertical distance of 69.8 m (every four rows of pillars). In the eastern coal panel, the sensors form a four-by-four grid with the eastern-most columns of sensors separated (horizontally) by two rows of pillars while the three western-most columns of sensors are separated by three rows of

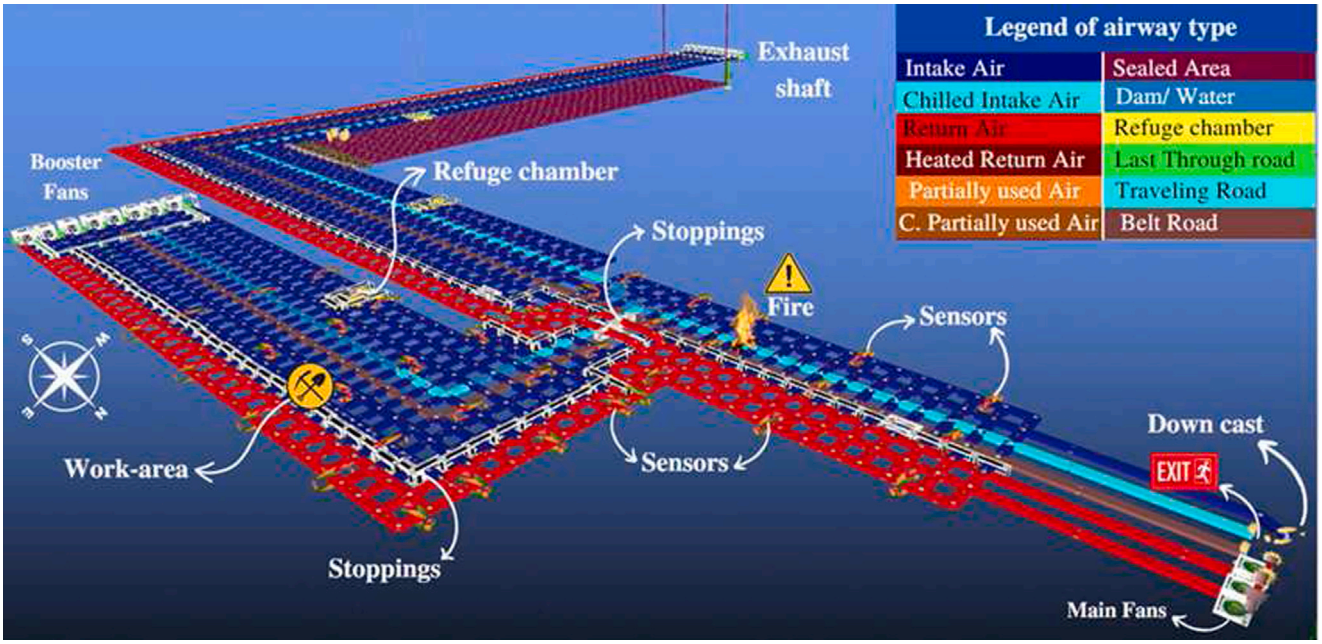

Fig. 1. VentSim™ DESIGN model for an underground coal mine.

pillars. The four rows of sensors in the eastern coal panel are separated (vertically) by four rows of pillars. The sensors form a denser mesh over the return air pathways compared to the rest of the panel since these pathways are by design (of the ventilation system) intended to serve as the safest escape routes. In the western coal panel, the sensors form a five by three grid. The columns of the sensors are separated (horizontally) by three rows of pillars, while the rows are separated (vertically) by four rows of pillars. The locations of the thirty-one (31) sensors cover the focus area sufficiently and allow for modeling multiple escape routes. An additional sensor is added at the exit of the mine to the surface (sensor 32) to allow modeling the endpoint of the escape routes. The working area coincides with the position of sensor 6, and thus this node models the start-point of the escape routes. The positioning and enumeration of the sensors on the VentSim™ DESIGN model are illustrated in Fig. 2.

The monitored parameters are a subset of the parameters available in the VentFIRE™ tool. The selected parameters allow for monitoring critical hazards that miners face during a fire evacuation: velocity of the airflow (m/s), carbon monoxide concentration (ppm), oxygen concentration (%), wet bulb temperature (°C), and visibility (m).

3.3. Fire simulation

According to Brake (2013), the fire chemistry and characteristics (fuel, burning rate, produced fumes) and the fire dynamics (growth and decay stages) are dependent on the amount of fresh air reaching the fire (Chen et al., 2003). To execute the fire simulation the following were assumed and input to the VentFIRE™ tool:

- The fire is caused by equipment malfunction/mishandling: mobile diesel equipment fire accident; mine truck MT2010, with tramming coal capacity of 20 000 kg and fuel tank capacity of 379 liters
- The burning substance is diesel combined with coal; the mine truck was carrying 50% of its capacity (10 000 kg); the fuel tank was full
- The fire occurred due to a vehicle rollover; the diesel spilled 50% of the truck tank (190 liters) on the floor
- The fire cannot be extinguished with onboard suppression system or portable extinguishers
- The duration of the fire is 1 h with a delay of fire start is 5 min, both the growth and the decay periods are 30 min

3.4. Ford-Fulkerson algorithm

The fire simulation results are used to quantify the risk for various locations in the mine during a fire emergency. The risk values are the inputs of a Ford-Fulkerson algorithm (FFA) that outputs viable escape routes. The FFA is a maximum-flow, minimum-cost flow (MFMC) optimization algorithm that computes the pathways for sending the maximum amount of flow through the network (Ford and Fulkerson, 1956; Neumann, 1984). A fire emergency creates two flows: (a) the flow of the fumes, reduction of fresh air, and heat; and (b) the flow of the mine worker's evacuation. Naturally, the evacuation routes (second flow) are highly dependent on the flow of the fire hazards (first flow - e.g., toxic gases and fumes, high heat, lack of fresh air, reduced visibility). Both flows share the same network (the mine entries and crosscuts), and conflicts can potentially arise where the evacuation flow overlaps the flow of highly hazardous conditions (Cui et al., 2014). In an emergency, real-time information about the distribution of the fire-induced hazards can help identify high-risk paths; thus, help find evacuation routes that do not jeopardize the health and lives of the mine workers.

In this study, the proposed approach formulates the first flow (i.e., the fire-induced hazards) into a MFMC problem based on the fire simulation results, to identify viable evacuation route for the miners from the workplace (source) to the surface (sink). The objective of the problem is to minimize the risk associated with an evacuation route.

The mathematical model of the problem is based on graph theory as follows: Let $G = (N, E)$ be a directed graph with the set of nodes N and the set of edges E. The graph G represents the network of entries and crosscuts of the underground mine. The nodes, $i \in N$, are the junctions

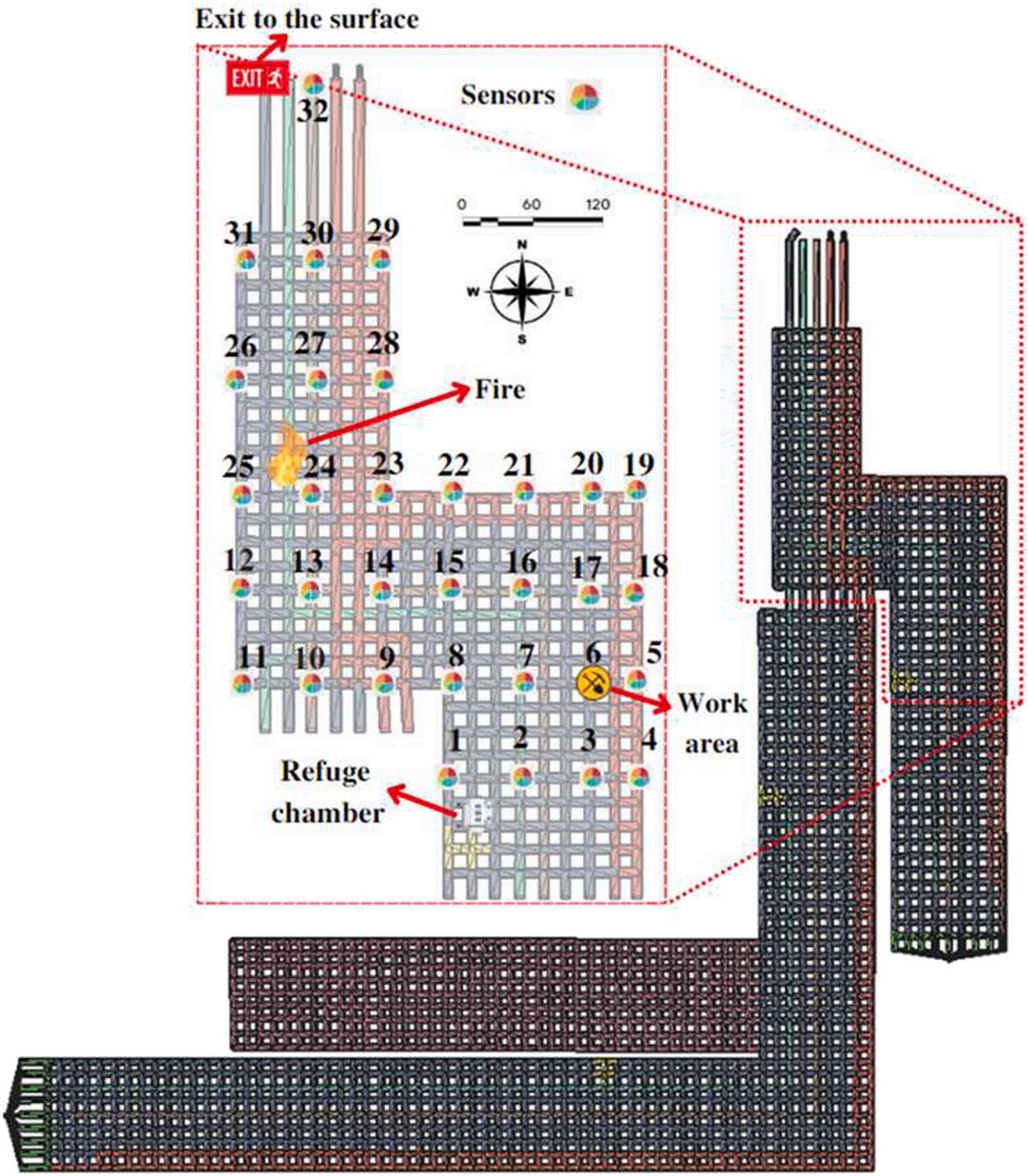

Fig. 2. Section of the mine used in simulated evacuation routes.

between the entries and the crosscuts, while the edges, $(i, j) \in E$, are the uninterrupted parts of the entries and crosscuts of the mine (also called airways). The size of the node sets is n and the size of the edges set is m, where $m \geq (n-1)$. A pair of connected nodes, (i, j), denote the endpoints of an edge. Each edge of the graph is associated with a cost value, $f(i, j)$. The cost of an edge has a different meaning that depends on the application, e.g., the distance from point i to point j, the time associated with traversing that edge, the energy consumption required to traverse that edge. In MFMC problems, each edge of the graph is also associated with a capacity value, $c(i, j)$, that represents the maximum

allowable flow for the edge. The edges that do not exceed this capacity value, i.e., $c(i,j) - f(i,j) > 0$, form a residual network, G_r, where all edges can allow flow (Ford and Fulkerson, 1956; Goldberg and Tarjan, 1988; Lavrov, 2020).

In this study, the cost is the fire-induced quantified risk for a mine worker at a given moment. The higher the combined fire-induced risks for a location of the mine, the higher the cost for the corresponding edge. If an edge exhibits a maximum allowable cost (capacity) or ceases to exist (e.g., because of a roof fall) then $f(i,j) = \infty$. The capacity of an edge of the evacuation route represents the maximum permissible hazard that a miner can sustain without irreversible health damage or death. In the proposed formulation, the cost associated with each risk is normalized to the range of $[0,1]$, and thus it follows that the capacity is equal to 1. In other words, the flow of the combined fire-induced hazards is analyzed to compute the eligible escape routes. Therefore, the FFA computes all the safe evacuation routes from the input graph that lead from the workplace (source node, s) to exit to the surface (sink node, t). The available evacuation routes are defined by the cost, $f(i,j)$, and the capacity, $c(i,j)$. If the cost does not reach or exceed the capacity of an edge, $c(i,j) - f(i,j) > 0$, escape through that edge is feasible. If the residual capacity of the edge becomes zero, $c_r(i,j) = 0$, then escape through that edge is not feasible and the edge is removed from the graph, $(i,j) \notin E$. During the execution of the iterative steps of the FFA, the flow of the combined risk $f(i,j)$ for each edge must satisfy the following constraints:

$$0 \le f(i,j) \le c(i,j) \quad \forall (i,j) \in E \tag{1}$$

$$f(i,j) = -f(j,i) \quad \forall (i,j) \in E \tag{2}$$

$$\sum_{u \in N} f(i,j) = 0 \quad \forall\, i,j \in N/s,t \tag{3}$$

$$\sum_{(s,i) \in E} f(s,i) = \sum_{(j,t) \in E} f(j,t)\,. \tag{4}$$

The capacity constraint, Eq. (1), prevents the flow from exceeding the capacity, i.e., the maximum permissible cost. The anti-symmetric constraint, Eq. (2), eliminates the possibility of having positive flow in both directions simultaneously. This is necessary because flow through and edge can occur both ways. Finally, the flow conservation, Eqs. (3) and (4) ensures that the net flow entering each node is zero, except for the source and the sink, while the flow leaving from the source must be equal to the flow arriving at the sink (Ford and Fulkerson, 1963). The pseudo-algorithm of the classic FFA is shown below:

Algorithm 1 Ford-Fulkerson Algorithm (G)

```
Initialize flow f to zero
for each edge (i, j) ∈ E do
    f(i, j) ← 0
end for
Use graph search algorithm to find all possible paths from s to t in G_r
for each path p : s → t ∈ G_r do
    c_r(p) ← min c_r(i, j) : (i, j) ∈ p
    for each edge (i, j) ∈ p do
        if (i, j) ∈ E then
            f(i, j) ← f(i, j) + c_r(p)
        else
            f(j, i) ← f(j, i) − c_r(p)
        end if
    end for
end for
```

where: $f(i,j)$ is the quantified risk for the edge (i,j), s is the initial node (source), t is the end-node (sink), and c_r is the residual capacity.

Additionally, in this study the implemented FFA is developed to return only the shortest paths, which lead from a source to a sink. This approach provides evacuation routes that are optimized regarding three parameters (in order of highest to lowest priority): (a) incremental risk, i.e., safety of individual edges/pathways, (b) overall distance of escape route, and (c) overall risk of escape route. This means that the FFA is less sensitive to the magnitude of the accumulated exposure to risk associated with the entirety of a valid pathway. The solution to this inherent flaw of the implemented FFA is to apply an evaluation processing to the output pathways. The total residual capacities of all the incrementally safe evacuation routes, which are calculated and stored during the execution of the FFA, can be used to find the pathways with the lower overall risk. The FFA is implemented in Python programming language (Python 3.7) and uses primarily the *networkx* library.

3.5. Risk quantification

The fire simulation, as executed through VentFIRE™, allows for obtaining the spatiotemporal distribution of the individual parameters of interest. Although the simulation software has the capability of estimating the optimum evacuation routes based on a user-selected parameter, the user cannot specify the safety criteria for evacuation purposes. The proposed approach allows the user to select these criteria, as well as define the combination of the individual parameters into one parameter. This compact parameter quantified the cumulative fire-induced hazards for any position in the mine. However, the individual parameters need to be normalized before combined. Normalizing the data allows for comparing and combining elements of different variables and units of measurement. Feature scaling, also called the min–max scaling method was employed to normalize the parameters to standardize their values and be able to combine the individual normalized data into one matrix (Aminossadati and Hooman, 2014; Nevill and Holder, 1995; Hamacher and Tjandra, 2001). The method uses the maximum and minimum values for each parameter and calculates the standard amount to combine the parameters. Eq. (5) represents the normalized value for each parameter:

$$P_n = \frac{P - P_{min}}{P_{max} - P_{min}} \tag{5}$$

where: P_n the normalized value of the parameter, P the raw value of the parameter, P_{min} the minimum value of the parameter, and P_{max} the maximum value of the parameter. The maximum and minimum values are defined based on the permissible standards proposed by MSHA. Note that if the original value, P, falls into the range of $[P_{min}, P_{max}]$, then the normalized value, P_n, will fall inside of the range of [0,1]. In this case, the boundaries are enforced to the normalized value so that $P_n \in [0,1]$ is always true. In some cases, though, the permissible limits by MSHA regulations may be either a maximum or a minimum limit, and not a range. In these cases, the normalized risk value is 0 if the permissible limit is respected, and 1 otherwise:

$$P_n = \begin{cases} 0, & \text{if } P \le P_{max} \text{ or } P \ge P_{min} \\ 1, & \text{otherwise.} \end{cases} \tag{6}$$

Subsequently, Eq. (7) is applied for combining the individual normalized parameters into the cost value that represents the combined risk for the health of a miner:

$$f(i,j) = \sum_{k=0}^{n_p} \lambda_k \; P_{n_k}(i,j) \tag{7}$$

where: f is the cost value, k is the number of the individual parameters of interest, λ_k are the weights for the individual parameters, and P_{n_k} are the normalized values for each parameter. If the individual risks are assumed to contribute in different proportions to the overall risk, the weights, λ_k, will not be equal, while, otherwise, the weights are equal.

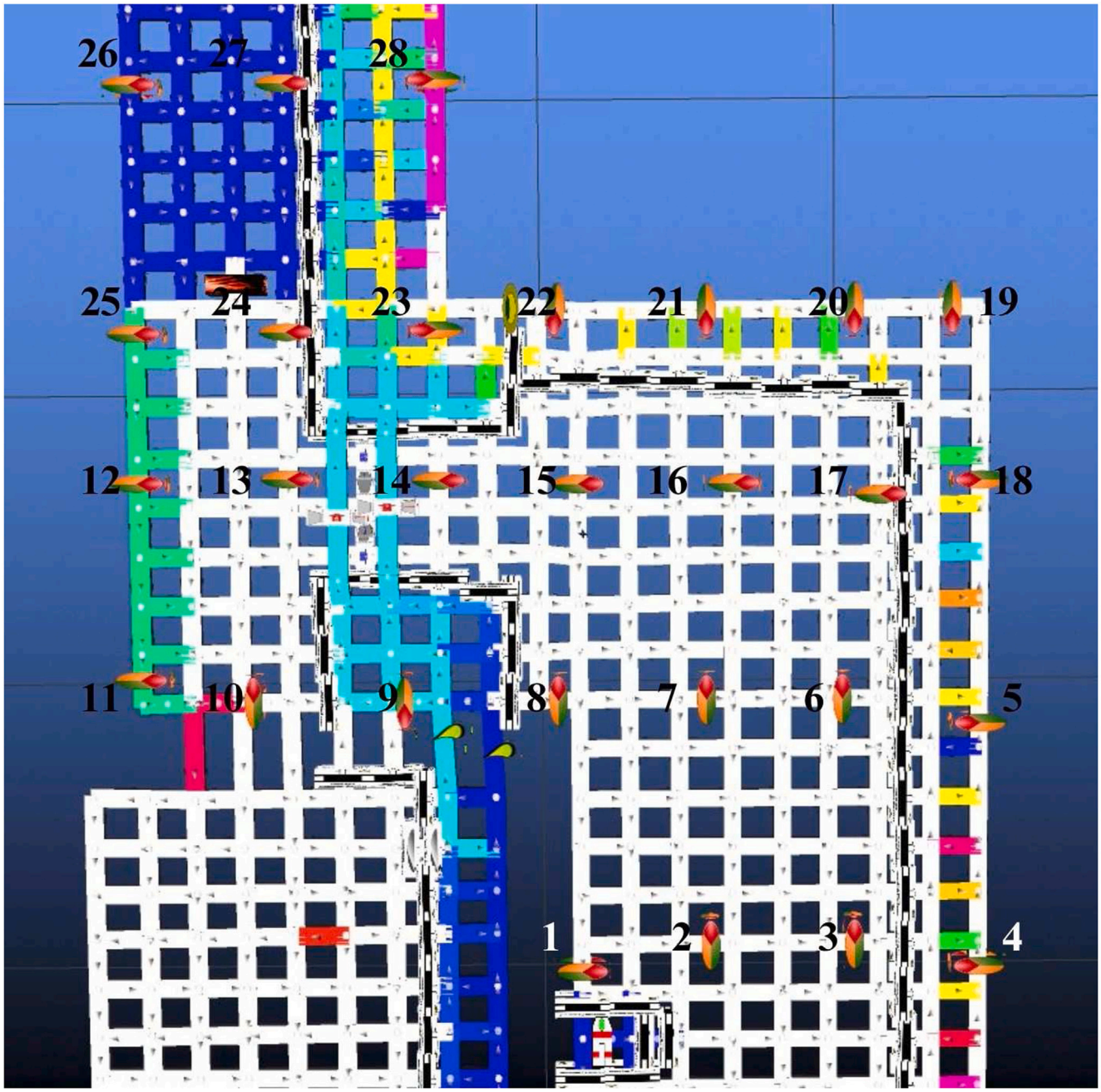

Fig. 3. Detail view of simulated sensors and ventilation curtains in the vicinity of the overcast air ducts.

Table 1
Airflow velocity simulation results in m/s as recorded by 18 of the sensors during 1 h of simulation.

Time (s)	9	11	13	23	24	25	27	29	31	1	3	5	6	7	15	17	19	21
1	1.8	0.9	1.8	1.8	2.1	2.1	2.1	2.7	2.1	0.3	0.1	1.8	0.4	0.2	0.2	0.2	0.9	1.8
300	1.8	0.9	1.8	1.8	2.1	2.1	2.1	2.7	2.1	0.3	0.1	1.8	0.4	0.2	0.2	0.2	0.9	1.8
600	1.8	0.9	1.8	1.8	2.1	2.1	2.1	2.7	2.1	0.3	0.1	1.8	0.4	0.2	0.2	0.2	0.9	1.8
900	1.8	0.9	1.8	1.8	2.2	2.2	2.1	2.7	2.1	0.3	0.1	1.8	0.4	0.2	0.2	0.2	0.9	1.8
1200	1.8	0.9	1.9	1.8	2.2	2.2	2.1	2.7	2.1	0.3	0.1	1.8	0.4	0.2	0.2	0.2	0.9	1.8
1500	1.8	0.9	1.9	1.8	2.3	2.3	2.1	2.7	2.1	0.3	0.1	1.8	0.4	0.2	0.2	0.2	0.9	1.8
1800	1.8	0.9	1.9	1.8	2.4	2.3	2.1	2.7	2.1	0.3	0.1	1.8	0.4	0.2	0.2	0.2	0.9	1.8
2100	1.8	0.9	2.0	1.8	2.4	2.3	2.1	2.7	2.1	0.3	0.1	1.8	0.4	0.2	0.2	0.2	0.9	1.8
2400	1.8	0.9	2.0	1.8	2.4	2.3	2.1	2.7	2.1	0.3	0.1	1.8	0.4	0.2	0.2	0.2	0.9	1.8
2700	1.8	0.9	2.0	1.8	2.4	2.3	2.1	2.7	2.1	0.3	0.1	1.8	0.4	0.2	0.2	0.2	0.9	1.8
3000	1.8	0.9	2.0	1.8	2.4	2.3	2.1	2.7	2.1	0.3	0.1	1.8	0.4	0.2	0.2	0.2	0.9	1.8
3300	1.8	0.9	2.0	1.8	2.4	2.3	2.1	2.7	2.1	0.3	0.1	1.8	0.4	0.2	0.2	0.2	0.9	1.8
3600	1.8	0.9	2.0	1.8	2.4	2.3	2.1	2.7	2.1	0.3	0.1	1.8	0.4	0.2	0.2	0.2	0.9	1.8

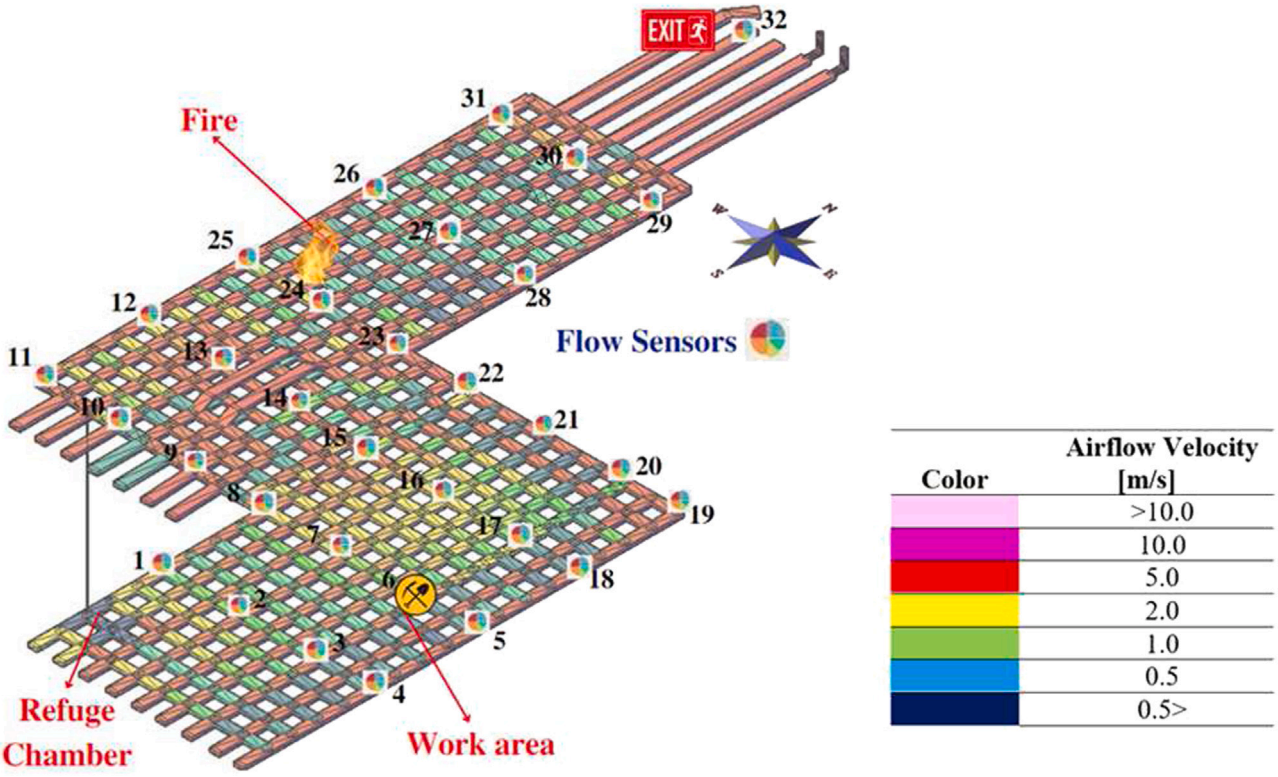

Fig. 4. Fire simulation of the velocity of the airflow after 1 h of simulation. (For interpretation of the references to color in this figure legend, the reader is referred to the web version of this article.)

Table 2
Temperature wet bulb results in °C as recorded by 18 of the sensors during 1 h of simulation.

Time (s)	9	11	13	23	24	25	27	29	31	1	3	5	6	7	15	17	19	21
1	20.8	21.3	21.3	21.0	21.2	21.3	21.2	21.2	21.2	21.2	21.2	21.5	21.1	21.2	21.4	21.1	21.5	21.5
300	20.8	21.1	21.2	21.1	21.1	21.1	21.1	21.2	21.1	21.3	21.2	21.5	21.1	21.2	21.1	21.1	21.5	21.5
600	20.8	21.0	22.1	21.0	21.1	21.1	21.1	21.2	21.1	21.0	21.1	21.5	21.1	21.0	21.3	21.1	21.5	21.4
900	20.8	21.1	23.9	21.0	21.4	21.1	21.1	21.2	21.1	21.2	21.0	21.5	21.0	21.2	22.1	21.0	21.5	21.4
1200	20.8	21.0	26.2	21.0	22.3	21.1	21.1	21.2	21.1	22.0	21.3	21.5	21.0	22.1	23.5	20.9	21.5	21.4
1500	20.8	21.1	28.3	21.0	23.6	21.2	21.1	21.2	21.1	23.4	22.3	21.5	21.4	23.6	25.1	21.2	21.5	21.4
1800	20.8	21.2	30.4	21.0	25.2	21.4	21.1	21.2	21.1	24.9	23.5	21.5	22.3	25.1	26.8	22.0	21.5	21.4
2100	20.9	21.4	31.9	21.1	26.3	21.6	21.1	21.2	21.1	26.4	24.7	21.5	23.4	26.7	28.6	23.1	21.5	21.4
2400	20.9	21.4	32.2	21.1	26.5	21.6	21.1	21.2	21.1	27.8	25.9	21.6	24.4	28.1	29.2	24.0	21.5	21.4
2700	20.9	21.5	32.4	21.1	26.6	21.6	21.1	21.3	21.1	28.4	26.9	21.8	25.4	28.6	29.3	25.0	21.7	21.6
3000	20.9	21.5	32.6	21.3	26.7	21.6	21.1	21.5	21.1	28.5	27.2	22.4	25.9	28.8	29.4	25.6	22.1	21.9
3300	20.9	21.5	32.7	21.4	26.9	21.6	21.1	21.7	21.1	28.6	27.3	22.7	26.1	28.9	29.6	25.8	22.5	22.3
3600	20.9	21.5	32.8	21.5	26.9	21.7	21.1	21.8	21.1	28.7	27.4	22.7	26.2	29.0	29.6	25.9	22.5	22.4

4. Results

In this section, the results of the fire simulation and the implemented FFA are presented and discussed. The preliminary analysis of the fire simulation data presented discusses the data of 18 out of the 33 simulated sensors; 16 out of the 18 selected sensors lie on a grid similar to the grid of the 33 sensors but has a doubled size (i.e., every other sensor was selected); the sensors on the fire spot and the working area were added, i.e., sensors 6 and 24. The 18 sensors are representative of the ventilation patterns. Nevertheless, the FFA analysis includes the data of all 33 sensors.

4.1. Fire simulation results

The fire simulation, as described above, is executed in VentSim™ DESIGN and the 'installed' sensors collect the data for the five selected parameters. The fire simulation is executed five times to obtain the results of the simulation for each parameter. The simulated fire event lasts 1 h (not to be confused with the running time of the software). Although the software can compute the sensor data every second, the results are chosen to be stored with an interval of 5 min (300 s) to reduce the amount of data. This simplification does not affect the results since all the parameters exhibit either constant or monotonic behavior (see data tables below). The values measured by the thirty-two sensors are collected and used for the subsequent analysis steps. The 2D

visualization of the final state of the mine, as provided by VentFIRE™, is obtained. The 2D colored maps illustrate the range of the measurements throughout the mine after the end of the fire simulation. If the upper limit of the color-bars is exceeded, a gray color is assigned to the area of the map by default. The upper limits of the color-bars were selected to be higher than the MSHA safety limits to obtain a better insight regarding the propagation of the fire-induced conditions.

4.1.1. Airflow velocity, v

Airflow velocity in airways where personnel work or travel must not be lower than 0.3 m/s. On the other side, excessive velocities can exacerbate problems of dust, breathing discomfort, and intensify fires. A typical value for working faces is between 1 and 3 m/s (Belle, 2013). Fig. 4 shows the airflow velocity map of the mine after the end of the fire simulation, while Table 1 contains the data collected by 18 of the sensors during the simulation (see all the data collected in Appendix). The sensor measurements show constant velocities throughout the mine, which is a desirable condition for a ventilation system. In general, the airflow velocity satisfies the lower limit for all the parts of the mine where workers work or travel. The inactive part of the coal panel (sensors 1 and 3) is intentionally provided with less amount of fresh air (and at slower speeds). Sensors 7, 15, and 17 measure low velocities because they are located next to the ventilation curtains (see Fig. 1). Finally, it should be noted that the velocities recorded by sensor 10 exhibit an atypical behavior that is not consistent with the readings of the adjacent (bilaterally) sensors 9 and 11. This happens because of the overcast air ducts as well as the ventilation curtains (stoppings) the isolate sensor 9 from the adjacent sensors (see Fig. 3).

4.1.2. Temperature wet bulb, T_{wb}

The wet bulb temperature measures the heat in mine environment that exceeds a wet bulb globe temperature of 79 °F (26 °C). Statistically, the highest accident rates are related to temperatures above 80 °F (27 °C) (US Department of Labor and MSHA and National Mine Health and Safety Academy, 2012). In this simulation, the temperature generated solely by the fire (and not the machinery or other sources) is measured. Fig. 5 shows the temperature wet bulb map of the mine after the end of the fire simulation, while Table 2 contains the data collected by 18 of the sensors during the simulation (see all the data collected in Appendix). Sensor 13 records temperatures higher than 27 °C after 25 min., as well as the highest temperatures throughout the simulation since it is the first one that receives the fire heat waves. Sensors 1, 3, 7, and 15 record significant increases in the temperature that exceed 27 °C after 35 min. after the fire started. The affected sensors receive the fire heat waves that propagate alongside the airflow direction (i.e., north to south and east to west). Note that sensor 24, which is the closest to the fire, never records temperatures higher than 26.9 °C because the airflow does not force the heat waves to propagate horizontally as much as it does vertically. The remaining sensors record constant temperatures less than 25.9 °C. Finally, the temperature recording from sensors 17, 19, 21, 23, 27, and 29 indicate that escape through the return air pathways would be safe even after 1 h after the fire started.

4.1.3. Carbon monoxide, CO

The most common cause of death in mine fire emergencies is carbon monoxide poisoning. The severity of symptoms caused by CO exposure in underground mines is determined by three main factors: the concentration of CO in the confined environment; exposure time, and workload and breathing rate (United Nations Environment Programme and World Health Organization, 1972; World Health Organization, 1979). Table 3 shows the quantity of CO, the allowable exposure time, and the symptoms produced per exposure level. According to the current legislation, the short-term exposure limit to CO in coal mines is 75 ppm for 15 min without proper approved respiratory protection (Occupational Safety and Health Administration (OSHA), 2012; US Department of Labor and MSHA, 2007). In this study, the worst-case scenario where the miners do not have proper respiratory protection is considered. Fig. 6 shows the CO concentration map of the mine after the end of the fire simulation, while Table 4 contains the data collected by 18 of the sensors during the simulation (see all the data collected in Appendix). Similarly to the propagation of the heat waves, the CO concentration increases rapidly along the south-bound vertical entries of the western coal panel and the east-bound horizontal crosscuts that connect the western and the eastern coal panels. Sensor 13 records a CO concentration of 89.5 ppm within 10 min after the fire started, while sensor 15 records a CO concentration of 166.8 ppm within 15 min. Note that sensor 24 records a CO concentration of more than 75 ppm after 15 min. Subsequently, the CO fumes move further inside the mine and the CO accumulation at the west part of the active coal panel (refuge chamber location) exceeds the safety limit between 15 and 20 min after the fire started (sensors 1 and 7). This means that the workers would have approximately 25 min available to take shelter at the refuge chamber (without protective equipment). Sensor 6 (working area) records a CO concentration higher than the safety limit between 15 and 20 min after the fire started. However, the return air pathways of the mine do not record CO concentration higher than the limit before 40 min from the starting of the fire (sensors 5, 19, 21, 23, and 29). This means that the CO concentration would allow the miners to safely evacuate through the return air pathways up to 40 min after the fire occurs. The least affected part of the mine is the part that lies north of the fire (sensors 26–31), as the direction of the intake air forces the fire fumes towards the interior of the mine. It must be noted that in the case of carbon monoxide data, the raw simulation data are converted to a more appropriate variable before used in the FFA. Considering that the legislation defines the maximum permissible exposure to CO to be 75 ppm for 15 min, the raw data for CO concentration must be converted so that the exposure time is incorporated. According to Kriebel et al. (2007), a common metric for time-varying occupational risk, especially for irreversible effects, can be provided by the product of intensity and duration, namely exposure, i.e., $E_j = x_j \times t_j$. Therefore, a new parameter that represents the total exposure of a miner to the CO content of an airway for the time that the miner needs to traverse that airway is computed based on the raw data, the average velocity of the evacuees (assumed to be 1 m/s), and the distance of an airway, i.e., $CO_e = CO \times \Delta t\ (i,j) = CO \times d(i,j) \times v_{avg}$. It follows that the maximum permissible value for this individual risk parameter is $CO_{max} = 75\ \text{ppm} \times 900\ \text{s} = 67{,}500\ \text{ppm s}$.

4.1.4. Oxygen, O_2

The minimum percentage of oxygen in an underground mine environment is 20%. Oxygen concentrations below this value can have adverse physiological effects (Szurgacz et al., 2019; Kevin and Linda, 2011). Fig. 7 shows the O_2 concentration map of the mine after the end of the fire simulation, while Table 5 contains the data collected by 18 of the sensors during the simulation (see all the data collected in Appendix). The levels of oxygen drop below the permissible limit in a similar but slower pattern as the increase of CO concentration. The first sensors to record O_2 concentration lower than the limit are located exactly south of the fire and at the junction airways between the west and east coal panel (sensors 13 and 15) 35 min after the fire started. The refuge chamber area becomes unsafe at around the same time (sensors 1 and 7). Subsequently, the O_2 concentration at the working area becomes unsafe between 45 and 50 min after the fire starts (sensors 3, 6, and 17). However, the return air pathways remain safe even 1 h after the fire occurs (sensors 5, 19, 21, 23, and 29).

4.1.5. Visibility, Vis

Visibility depends on the amount of smoke dispersed in the mine. The smoke hinders the visibility of the miners when they are evacuating. Visibility below 5 m adversely affects the miners' escape since it hinders the miner's ability to evaluate hazards in proximity. Awareness between 5 and 10 m is critical for self-escape mines (Brake, 2013; Ryan

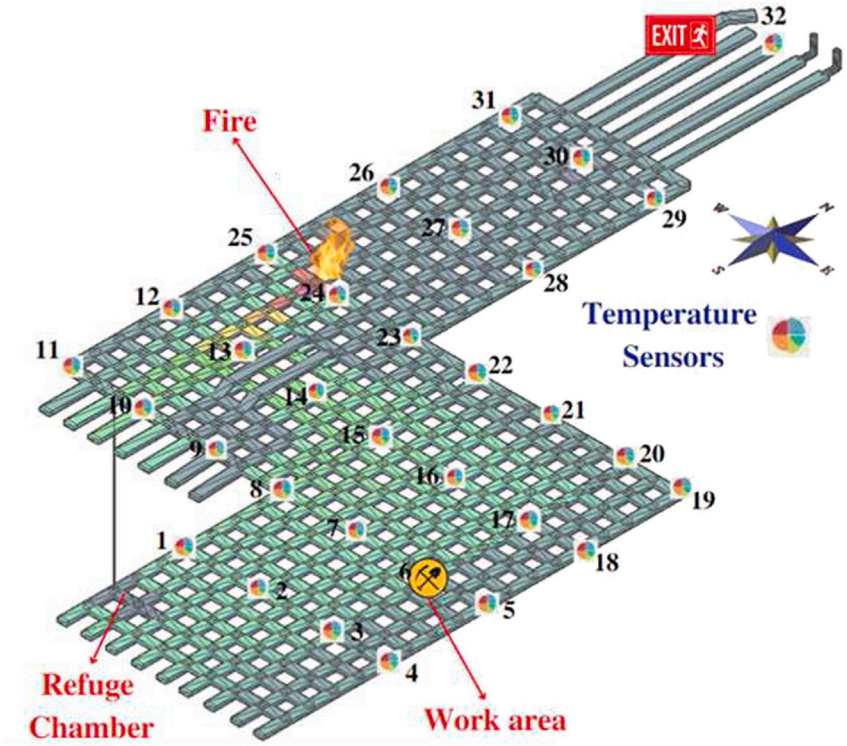

Color	Temp. Wet Bulb [°C]
	>60
	60
	50
	35
	25
	15
	15>

Fig. 5. Fire simulation of the temperature wet bulb after 1 h of simulation. (For interpretation of the references to color in this figure legend, the reader is referred to the web version of this article.)

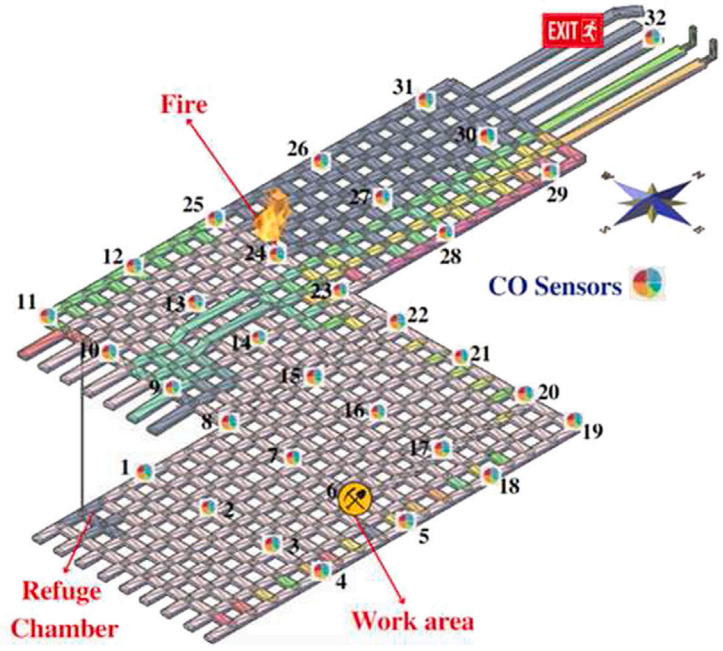

Color	Gas CO [ppm]	Time exposure [sec] With Protection	Time exposure [sec] Without protection
	>400	900	100
	400	10800	
	300	18000	300
	200		
	100	28800	900
	50		
	0		

Fig. 6. Fire simulation of the CO concentration after 1 h of simulation. The VentSim™ build-in exposure limits to CO fumes are presented next to the colorbar. (For interpretation of the references to color in this figure legend, the reader is referred to the web version of this article.)

Table 3
Health effects from exposure to CO levels in underground mines (US Department of Labor and MSHA, 2007).

Exposure level	CO level (ppm)	Time (h)	Symptoms
Minimum	1–70	8	Food poisoning and flu symptoms
Medium	150–300	5	Dizziness, vomiting, tinnitus, breathing difficulties, impaired judgment, confusion, drowsiness, memory loss, walking problems
Extreme	>400	3 to 4	Convulsion, coma, collapse, unconsciousness, brain damage, death

Table 4
Carbon monoxide concentration results in ppm as recorded by 18 of the sensors during 1 h of simulation.

Time (s)	9	11	13	23	24	25	27	29	31	1	3	5	6	7	15	17	19	21
1	0.0	0.0	0.0	0.0	0.0	0.0	0.0	0.0	0.0	0.0	0.0	0.0	0.0	0.0	0.0	0.0	0.0	0.0
300	0.0	0.0	8.3	0.0	0.0	0.0	0.0	0.0	0.0	0.0	0.0	0.0	0.0	0.0	0.5	0.0	0.0	0.0
600	0.0	0.0	89.5	0.0	1.6	0.0	0.0	0.0	0.0	0.9	0.0	0.0	0.0	1.9	35.2	0.0	0.0	0.0
900	0.2	0.0	282.5	0.0	33.6	0.0	0.0	0.0	0.0	51.9	0.0	0.0	0.6	60.0	166.8	0.7	0.0	0.0
1200	1.7	1.1	602.5	0.3	134.9	2.7	0.0	0.1	0.0	242.3	1.2	0.0	24.6	252.3	419.8	16.4	0.0	0.0
1500	5.1	12.4	1041.1	1.4	316.7	17.3	0.0	0.5	0.0	589.9	28.6	0.0	132.2	597.0	798.9	99.1	0.0	0.0
1800	10.5	37.4	1595.7	3.6	585.4	45.9	0.0	1.3	0.0	1094.6	139.8	0.2	361.7	1091.0	1295.6	290.7	0.0	0.0
2100	17.7	72.1	2044.2	7.4	792.7	77.3	0.0	2.9	0.0	1736.9	374.2	7.2	727.7	1719.8	1874.8	610.1	2.7	1.4
2400	26.5	81.2	2068.2	17.2	799.5	81.4	0.0	11.1	0.0	2464.9	747.2	45.9	1224.9	2402.8	2065.3	1055.1	26.6	18.5
2700	33.8	82.2	2069.7	43.9	802.8	82.4	0.0	44.0	0.0	2715.9	1255.4	146.7	1820.1	2605.5	2084.7	1594.7	101.4	79.2
3000	35.8	83.1	2070.9	97.7	805.9	83.4	0.0	122.2	0.0	2731.2	1848.4	335.5	2187.0	2622.5	2089.1	1982.6	255.0	211.9
3300	38.1	84.1	2072.6	188.7	809.0	84.3	0.0	263.5	0.0	2734.6	2219.9	628.8	2278.1	2627.1	2091.0	2068.2	506.8	437.8
3600	39.9	84.6	2073.5	248.9	810.4	84.8	0.0	358.7	0.0	2735.4	2301.2	814.8	2291.2	2628.1	2092.0	2082.1	669.6	585.2

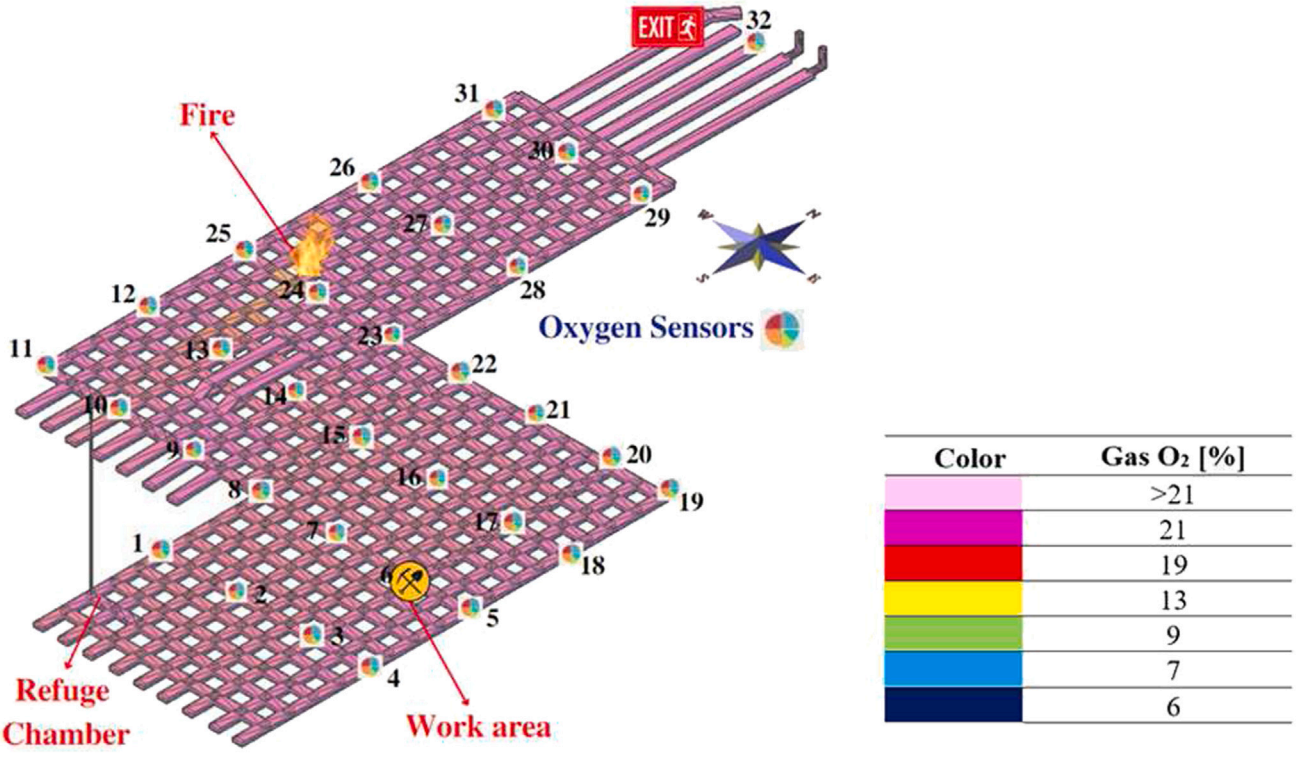

Fig. 7. Fire simulation of the O2 concentration in % percentage after 1 h of simulation. (For interpretation of the references to color in this figure legend, the reader is referred to the web version of this article.)

Table 5
Oxygen concentration results in % as recorded by 18 of the sensors during 1 h of simulation.

Time (s)	9	11	13	23	24	25	27	29	31	1	3	5	6	7	15	17	19	21
1	21.0	21.0	21.0	21.0	21.0	21.0	21.0	21.0	21.0	21.0	21.0	21.0	21.0	21.0	21.0	21.0	21.0	21.0
300	21.0	21.0	21.0	21.0	21.0	21.0	21.0	21.0	21.0	21.0	21.0	21.0	21.0	21.0	21.0	21.0	21.0	21.0
600	21.0	21.0	20.9	21.0	21.0	21.0	21.0	21.0	21.0	21.0	21.0	21.0	21.0	21.0	20.9	21.0	21.0	21.0
900	21.0	21.0	20.8	21.0	20.9	21.0	21.0	21.0	21.0	20.9	21.0	21.0	21.0	20.9	20.9	21.0	21.0	21.0
1200	21.0	21.0	20.6	21.0	20.9	21.0	21.0	21.0	21.0	20.8	21.0	21.0	20.9	20.8	20.7	21.0	21.0	21.0
1500	21.0	21.0	20.3	21.0	20.8	21.0	21.0	21.0	21.0	20.6	20.9	21.0	20.9	20.6	20.5	20.9	21.0	21.0
1800	21.0	20.9	20.0	21.0	20.6	20.9	21.0	21.0	21.0	20.3	20.9	21.0	20.7	20.3	20.1	20.8	21.0	21.0
2100	21.0	20.9	19.7	21.0	20.5	20.9	21.0	21.0	21.0	19.9	20.7	21.0	20.5	19.9	19.8	20.6	21.0	21.0
2400	20.9	20.9	19.7	21.0	20.5	20.9	21.0	21.0	21.0	19.4	20.5	20.9	20.2	19.5	19.7	20.3	20.9	21.0
2700	20.9	20.9	19.7	20.9	20.5	20.9	21.0	20.9	21.0	19.3	20.2	20.9	19.8	19.3	19.7	20.0	20.9	20.9
3000	20.9	20.9	19.7	20.9	20.5	20.9	21.0	20.9	21.0	19.2	19.8	20.8	19.6	19.3	19.7	19.7	20.8	20.8
3300	20.9	20.9	19.7	20.8	20.5	20.9	21.0	20.8	21.0	19.2	19.6	20.6	19.5	19.3	19.6	19.7	20.6	20.7
3600	20.9	20.9	19.7	20.8	20.5	20.9	21.0	20.7	21.0	19.2	19.5	20.4	19.5	19.3	19.6	19.7	20.5	20.6

Table 6
Visibility results in m (obstructed by smoke) as recorded by 18 of the sensors during 1 h of simulation.

Time (s)	9	11	13	23	24	25	27	29	31	1	3	5	6	7	15	17	19	21
1	25.0	25.0	25.0	25.0	25.0	25.0	25.0	25.0	25.0	25.0	25.0	25.0	25.0	25.0	25.0	25.0	25.0	25.0
300	25.0	25.0	25.0	25.0	25.0	25.0	25.0	25.0	25.0	25.0	25.0	25.0	25.0	25.0	25.0	25.0	25.0	25.0
600	25.0	25.0	24.9	25.0	25.0	25.0	25.0	25.0	25.0	25.0	25.0	25.0	25.0	25.0	25.0	25.0	25.0	25.0
900	25.0	25.0	9.0	25.0	25.0	25.0	25.0	25.0	25.0	25.0	25.0	25.0	25.0	25.0	20.8	25.0	25.0	25.0
1200	25.0	25.0	2.4	25.0	19.2	25.0	25.0	25.0	25.0	17.1	25.0	25.0	25.0	16.6	5.0	25.0	25.0	25.0
1500	25.0	25.0	1.1	25.0	5.2	25.0	25.0	25.0	25.0	3.2	25.0	25.0	23.7	3.2	1.7	24.2	25.0	25.0
1800	25.0	25.0	0.6	25.0	2.1	24.7	25.0	25.0	25.0	1.2	24.5	25.0	7.3	1.2	0.9	8.1	25.0	25.0
2100	25.0	18.0	0.4	25.0	1.1	14.4	25.0	25.0	25.0	0.6	8.7	25.0	2.2	0.6	0.5	2.4	25.0	25.0
2400	25.0	8.8	0.3	25.0	0.8	8.0	25.0	25.0	25.0	0.4	2.5	25.0	1.0	0.4	0.3	1.1	25.0	25.0
2700	23.1	7.6	0.3	24.9	0.8	7.6	25.0	25.0	25.0	0.3	1.1	16.0	0.6	0.3	0.3	0.6	21.6	23.8
3000	18.2	7.5	0.3	15.4	0.8	7.5	25.0	16.0	25.0	0.2	0.6	4.7	0.4	0.2	0.3	0.4	7.1	9.1
3300	17.2	7.4	0.3	6.7	0.8	7.4	25.0	5.5	25.0	0.2	0.4	2.0	0.3	0.2	0.3	0.3	2.6	3.2
3600	16.2	7.3	0.3	3.4	0.8	7.3	25.0	2.5	25.0	0.2	0.3	1.0	0.3	0.2	0.3	0.3	1.3	1.5

and Watkinson, 2017; Conti et al., 2005). Fig. 8 shows the visibility map of the mine after the end of the fire simulation, while Table 6 contains the data collected by 18 of the sensors during the simulation (see all the data collected in Appendix). The visibility deteriorates rapidly at the southern part of the entry of the fire, where sensor 13 records a value of 9 m after 10 min and of 2.4 m after 15 min after the fire started. After 20 min, the visibility drops below the safety limit at the refuge chamber area, as well as at the junction airways between the west and east coal panel (sensors 1, 7, and 15), while the area adjacent to the fire incident (sensor 24) becomes unsafe after 25 min. The working area (sensor 6) remains safe for 25–30 min after the fire started, as the ventilation curtains prevent the smoke propagating rapidly towards that area. The ventilation curtains keep the return air pathways clear from smoke for 45–50 min (sensors 5, 19, 21, 23, and 29).

4.2. Overview of simulation results

Figs. 9–12 show the data for the temperature (wet bulb), carbon monoxide, oxygen, and visibility as collected by 18 of the sensors along with the corresponding safety limits (red dotted lines). Based on these measurements, the preliminary conclusion is that the miners have approximately 20–25 min to enter the refuge chamber and approximately 35–40 min to evacuate towards the exit through the return air pathways of the mine.

4.3. Ford-Fulkerson algorithm analysis

A preliminary analysis that precedes the implementation of the FFA to the fire simulation data is required. This analysis, as explained earlier, includes data conversion (if needed), data normalization, and data combination. Note that a relatively high interval of five minutes (300 s) was selected for data collection from the sensors since the measurements show a monotonic behavior. However, this may not be true for different models and the values may exhibit fluctuations. The speed of the dynamic changes of these parameters depends on the geometry of the mine, the ventilation system, and the fire characteristics.

The possible evacuation routes of the simulated underground mine are modeled through nodes that denote the locations of the sensors in the ventilation model. Therefore, the input of the FFA algorithm is a graph consisting of 31 nodes (sensors positions), the position of the workspace as the source node, and the position of the exit to the surface as the sink node. The FFA is applied to this graph for twelve different time points after the simulated fire occurs (timestep of 5 min for a total of 1 h). The fire-induced health risks for each edge connecting the nodes/sensor are obtained based on the simulation data for these time points and the corresponding combined risk is computed for each edge of the graph. The FFA is executed for three different scenarios regarding the risks: (i) only high heat is present, (ii) only CO contamination is present, and (iii) combined risk stemming from the CO contamination, the reduction of O_2, the heat waves, and the reduced visibility.

The algorithm finds the shortest paths for each given time point based on the maximum capacity for the quantified fire-induced hazards. The escape routes, leading from the workspace to the exit of the mine, which exceed the maximum risk that the miners can withstand without irreversible health damage or death are discarded by the algorithm. The worst-case scenario of no availability of respiratory protective equipment for the miners is investigated. The implementation of the FFA is based on the following assumptions:

(a) Although the possible escape routes consist of every safe tunnel/airway in the mine, a sparser graph is selected to demonstrate the proposed approach. This simplification does not affect the results of the FFA. The advantage of this simplification is the reduced computational cost.

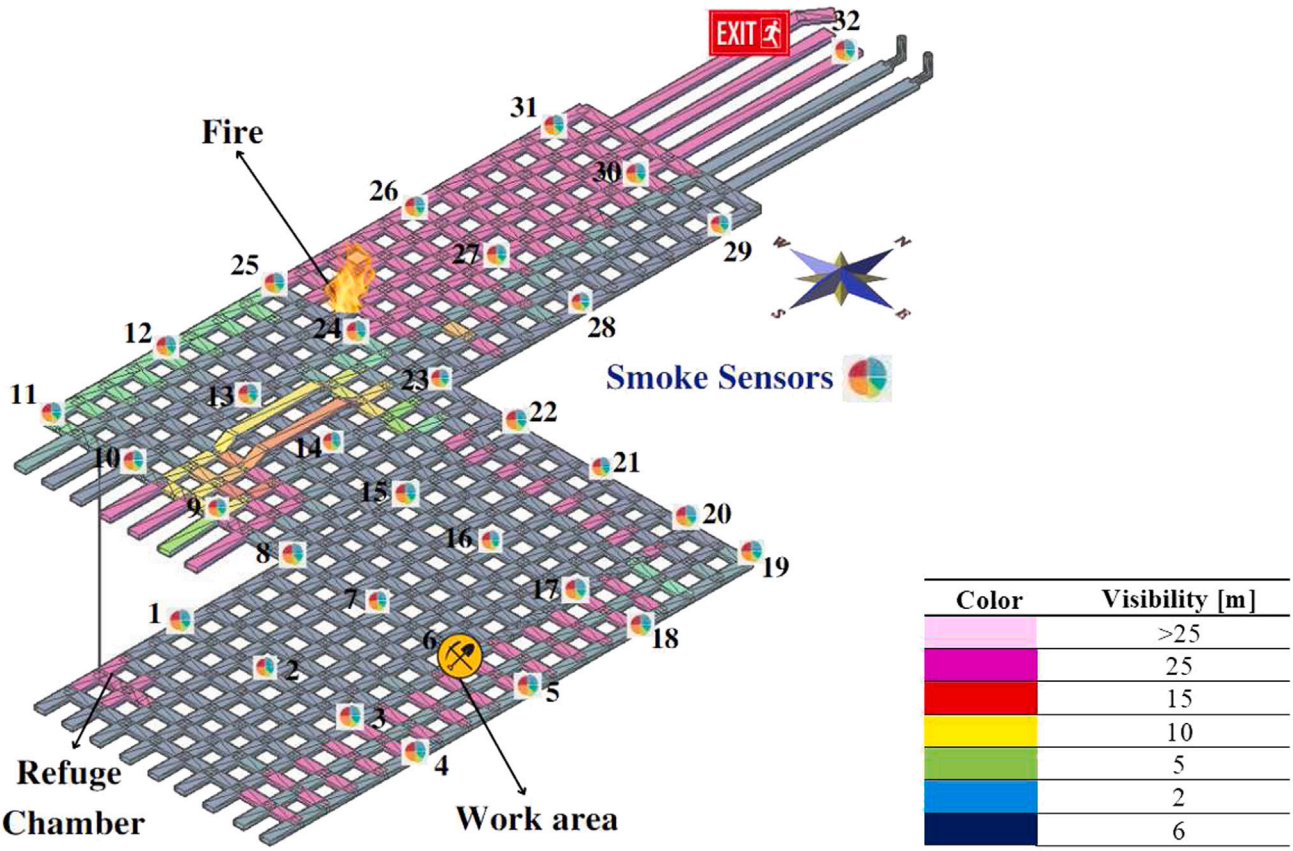

Fig. 8. Fire simulation of the visibility obstructed by the smoke in m after 1 h of simulation. (For interpretation of the references to color in this figure legend, the reader is referred to the web version of this article.)

Table 7
Cumulative risk and distance for optimum paths computed based on heat waves (T_{wb}).

Time (s)	Risk	Distance (m)
300	0.0, 0.0, 0.0	638.6, 638.6, 638.6
600	0.0, 0.0, 0.0	638.6, 638.6, 638.6
900	0.0, 0.0, 0.0	638.6, 638.6, 638.6
1200	0.0, 0.0, 0.0	638.6, 638.6, 638.6
1500	0.0, 0.0, 0.0	638.6, 638.6, 638.6
1800	0.0, 0.0, 0.0	638.6, 638.6, 638.6
2100	0.0, 0.0, 0.0	638.6, 638.6, 638.6
2400	0.0, 0.0, 0.0	638.6, 638.6, 638.6
2700	0.0, 0.0, 0.0	638.6, 638.6, 638.6
3000	0.0, 0.0, 0.0	638.6, 638.6, 638.6
3300	0.0, 0.0, 0.0	638.6, 638.6, 638.6
3600	0.0, 0.0, 0.0	638.6, 638.6, 638.6

(b) The VentSim™ DESING software allows the sensors to be anchored in the middle of the airways (i.e., the parts of the entries between two crosscuts). The endpoint of each monitored airway was used as the node of the graph, while the measurements of the corresponding sensor are assumed to be true for the entirety of the edges of the graph that end at that node. If a node can be assigned more than one value, the maximum value is selected.

(c) The capacity for the combined risk that determines whether an edge of the graph network is safe for the miners is set to be 1.00. This value is not derived by a specific natural quantity and can be changed according to the desired level of safety for the output escape routes. This value is selected based on the scenario that if one of the individual risks exceeds the corresponding safety limit, the normalized value for that location is equal to 1.00.

(d) In the implementation of the customized FFA routine, all the edges that start or end to the source or the sink nodes are considered for the creation of the safe graph networks even when the corresponding risk is greater than the capacity. This was selected for the purpose of gaining some insights regarding the optimal reaction times for the miners. The optimum routes for each individual time point during the 1 h simulation are computed with the assumption that the workers have not started evacuating from the work area before that time.

4.3.1. *Temperature wet bulb, T_{wb}*

Fig. 13 shows the three optimal evacuation routes during the fire emergency considering only the fire-induced heat waves to define the safety of the different pathways. Table 7 shows the cumulative risk and distance of the optimal paths, while Table 8 shows the statistics for all available shortest paths. On the contrary, Table 9 provides the total risk and distance of all viable paths, independently of the total length of the path (for comparative purposes).

4.3.2. *Carbon monoxide,* CO

Fig. 14 shows the three optimal evacuation routes during the fire emergency considering only the fire-induced carbon monoxide fumes to define the safety of the different pathways. Table 10 shows the cumulative risk and distance of the optimal paths, while Table 11 shows the statistics for all available shortest paths. On the contrary, Table 12 provides the total risk and distance of all viable paths.

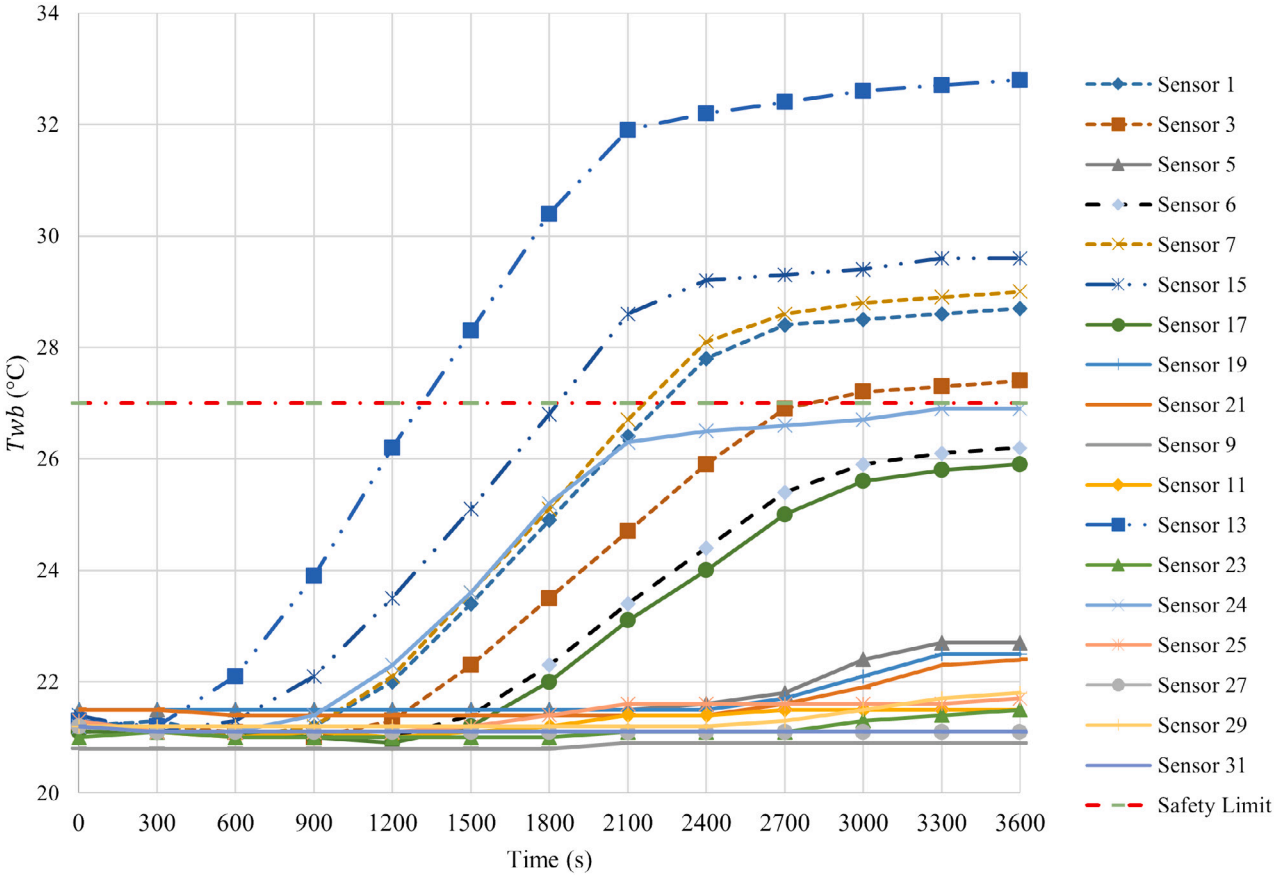

Fig. 9. Temperature (wet bulb) data collected from 18 of the sensors. (For interpretation of the references to color in this figure legend, the reader is referred to the web version of this article.)

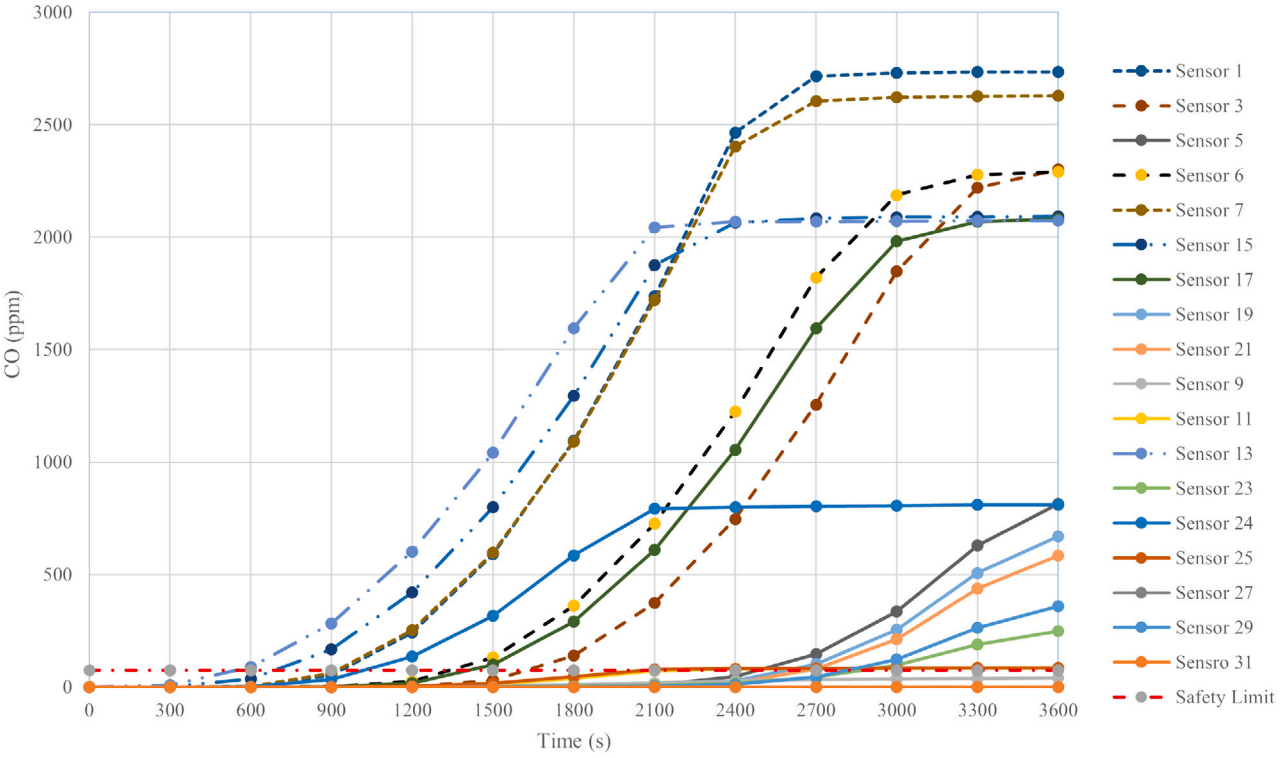

Fig. 10. Carbon monoxide concentration data collected from 18 of the sensors. (For interpretation of the references to color in this figure legend, the reader is referred to the web version of this article.)

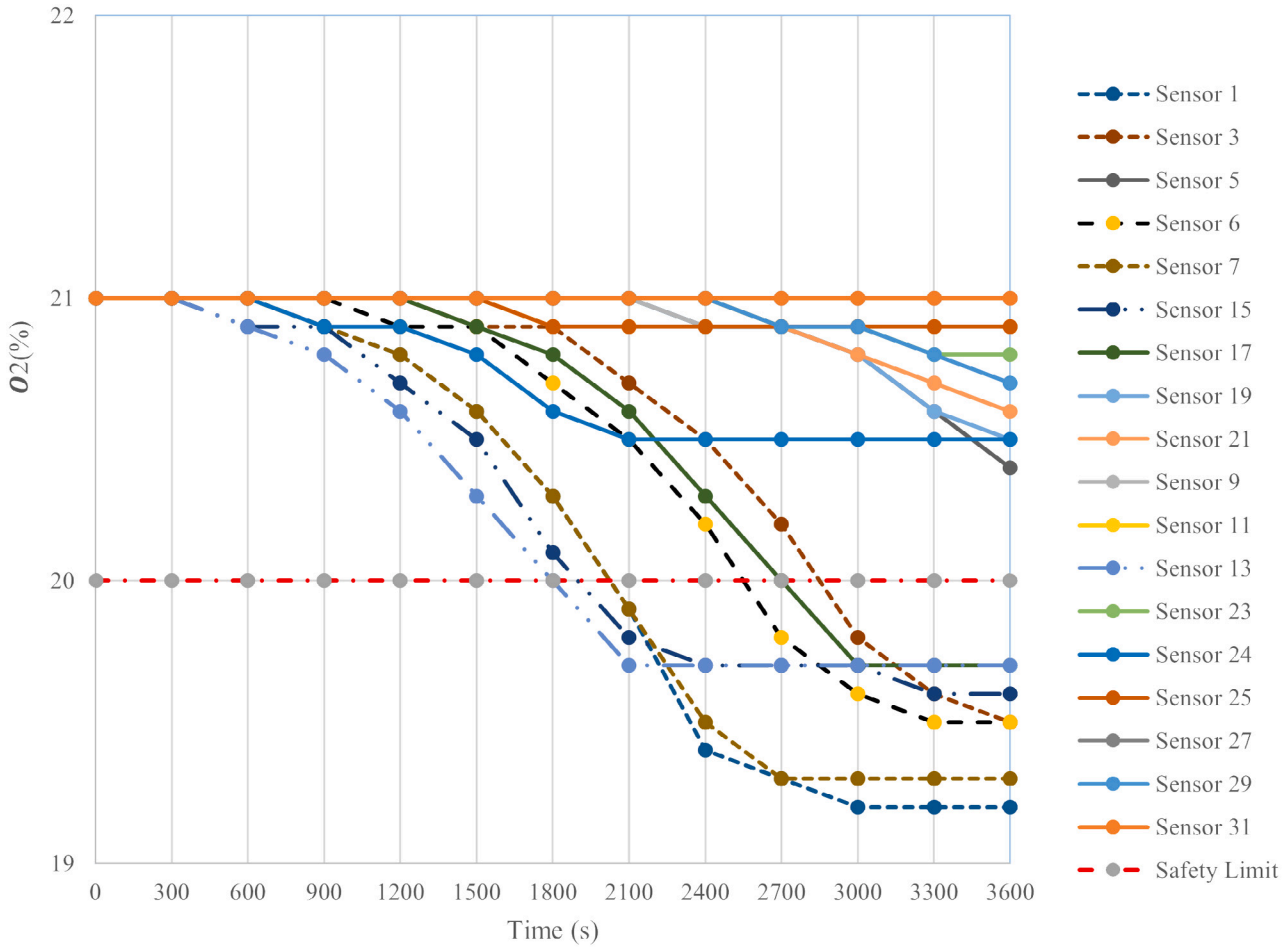

Fig. 11. Oxygen concentration data collected from 18 of the sensors. (For interpretation of the references to color in this figure legend, the reader is referred to the web version of this article.)

Table 8
Cumulative risk and distance for all shortest paths computed based on heat waves (T_{wb}).

Time (s)	No. of paths	Risk	Distance (m)
300	35	min: 0.0, max: 0.0, avg: 0.0	min: 638.6, max: 638.6, avg: 638.6
600	35	min: 0.0, max: 0.0, avg: 0.0	min: 638.6, max: 638.6, avg: 638.6
900	35	min: 0.0, max: 0.0, avg: 0.0	min: 638.6, max: 638.6, avg: 638.6
1200	35	min: 0.0, max: 0.0, avg: 0.0	min: 638.6, max: 638.6, avg: 638.6
1500	35	min: 0.0, max: 2.0, avg: 0.3	min: 638.6, max: 638.6, avg: 638.6
1800	35	min: 0.0, max: 5.0, avg: 1.8	min: 638.6, max: 638.6, avg: 638.6
2100	35	min: 0.0, max: 5.0, avg: 2.5	min: 638.6, max: 638.6, avg: 638.6
2400	35	min: 0.0, max: 6.0, avg: 3.8	min: 638.6, max: 638.6, avg: 638.6
2700	35	min: 0.0, max: 6.0, avg: 3.8	min: 638.6, max: 638.6, avg: 638.6
3000	35	min: 0.0, max: 6.0, avg: 3.8	min: 638.6, max: 638.6, avg: 638.6
3300	35	min: 0.0, max: 6.0, avg: 3.8	min: 638.6, max: 638.6, avg: 638.6
3600	35	min: 0.0, max: 6.0, avg: 3.8	min: 638.6, max: 638.6, avg: 638.6

4.3.3. Combined risk, T_{wb}-CO-O_2-Vis

Fig. 15 shows the three optimal evacuation routes during the fire emergency considering the heat waves, the carbon monoxide fumes, the reduction of fresh air (O_2), and the visibility obstruction caused by the fire to define the safety of the different pathways. Table 13 shows the cumulative risk and distance of the optimal paths, while Table 14 shows the statistics for all available shortest paths. On the contrary, Table 15 provides the total risk and distance of all viable paths.

4.4. Overview of graph network analysis

Fig. 13 shows the output evacuation routes for the first scenario. The heat waves propagate slowly towards the working area and the return air pathways. The optimal evacuation routes computed for this scenario go through the vicinity of the fire up to 20 min after the fire starts. During the next 15 min, slight detours are suggested to avoid the propagation of the heat waves, while 40 min after the fire starts the working area starts receiving the fire-induced heat waves and different shortest paths to the exit are suggested. During the remaining of the

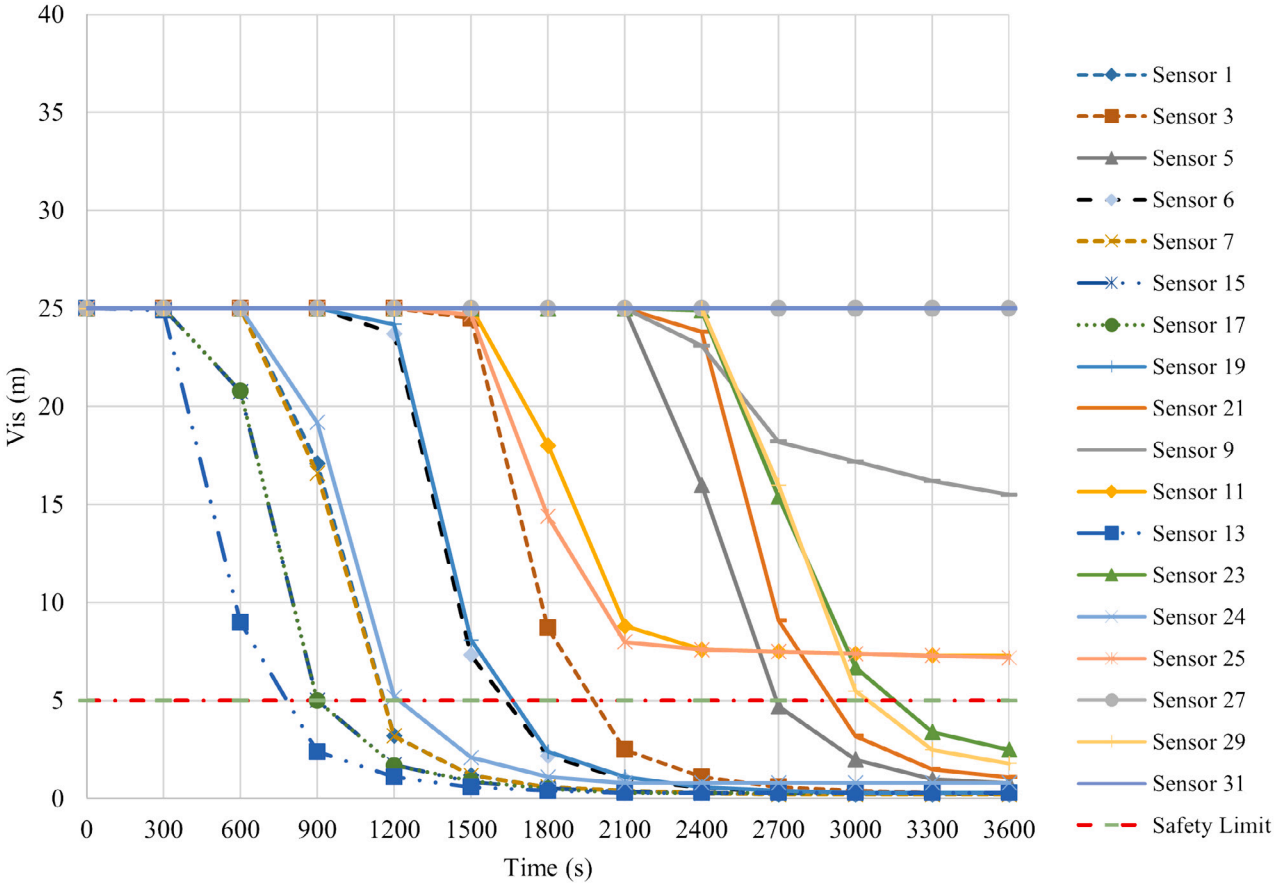

Fig. 12. Visibility data collected from 18 of the sensors. (For interpretation of the references to color in this figure legend, the reader is referred to the web version of this article.)

Table 9
Cumulative risk and distance for all possible paths computed based on heat waves (T_{wb}).

Time (s)	No. of paths	Risk	Distance (m)
300	32 359	min: 0.0, max: 0.0, avg: 0.0	min: 638.6, max: 1896.6, avg: 1311.5
600	32 359	min: 0.0, max: 0.0, avg: 0.0	min: 638.6, max: 1896.6, avg: 1311.5
900	32 359	min: 0.0, max: 0.0, avg: 0.0	min: 638.6, max: 1896.6, avg: 1311.5
1200	32 359	min: 0.0, max: 0.0, avg: 0.0	min: 638.6, max: 1896.6, avg: 1311.5
1500	32 359	min: 0.0, max: 2.0, avg: 1.6	min: 638.6, max: 1896.6, avg: 1311.5
1800	32 359	min: 0.0, max: 8.0, avg: 5.3	min: 638.6, max: 1896.6, avg: 1311.5
2100	32 359	min: 0.0, max: 10.0, avg: 6.1	min: 638.6, max: 1896.6, avg: 1311.5
2400	32 359	min: 0.0, max: 13.0, avg: 8.4	min: 638.6, max: 1896.6, avg: 1311.5
2700	32 359	min: 0.0, max: 13.0, avg: 8.4	min: 638.6, max: 1896.6, avg: 1311.5
3000	32 359	min: 0.0, max: 14.0, avg: 8.9	min: 638.6, max: 1896.6, avg: 1311.5
3300	32 359	min: 0.0, max: 14.0, avg: 8.9	min: 638.6, max: 1896.6, avg: 1311.5
3600	32 359	min: 0.0, max: 14.0, avg: 8.9	min: 638.6, max: 1896.6, avg: 1311.5

simulation (20 min), the suggested evacuation routes remain the same. During that period, the quantified risk stemming from the heat waves exceeds the maximum risk capacity close to the working area but does not cut off all the viable paths. This means that evacuation is feasible even after 1 h after the fire starts when only the heat waves risk is considered. The cumulative risk for the three paths computed for all the time-points is always equal to zero and the total distance is always the shortest possible, i.e., 638.6 m (Table 7). Table 8 shows that there are 32 additional shortest (i.e., total distance is 638.6 m) and safe paths for every time-point examined. However, the average cumulative risk of the 35 shortest paths starts increasing from 0.0 up to 6.0 after 20 min. Finally, Table 9 shows that there are 32,359 possible and safe paths (independently of total distance) for every time-point examined. The total distance of these paths can be as long as 1896.6 m, i.e., almost three times the distance of the shortest paths, while the cumulative risk raises up to more than twice the maximum cumulative risk of the shortest paths, i.e., 14.0 against 6.0.

Fig. 14 shows the output evacuation routes for the second scenario. The CO fumes propagate faster than the heat waves and pose a greater risk to the miners (as evidenced by the higher risk values). The optimal evacuation routes computed for this scenario go through the vicinity of the fire up to only 5 min after the fire starts, while after 10 min the fumes have contaminated the area west of the working area that

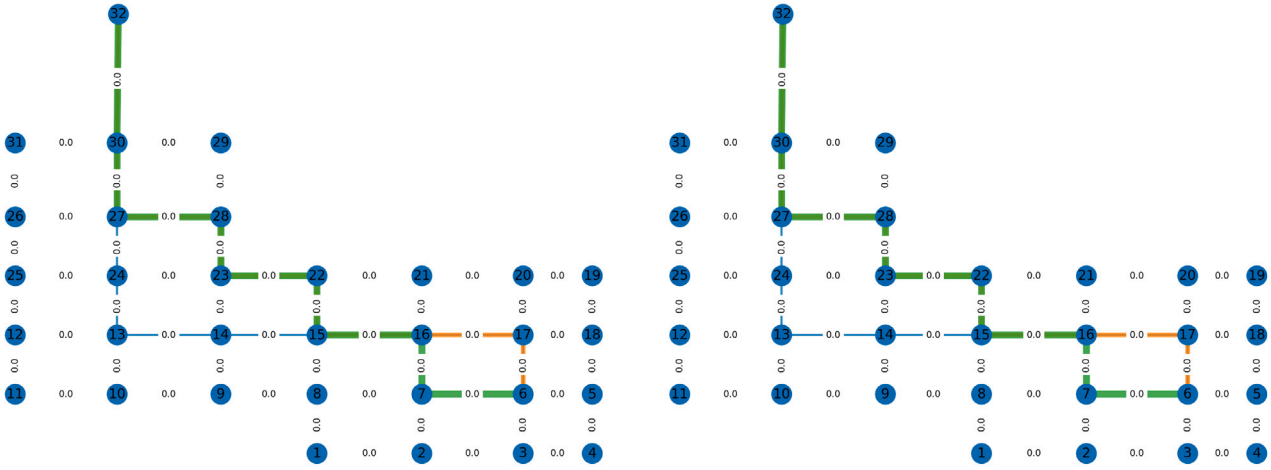

(a) 300 s (b) 600 s

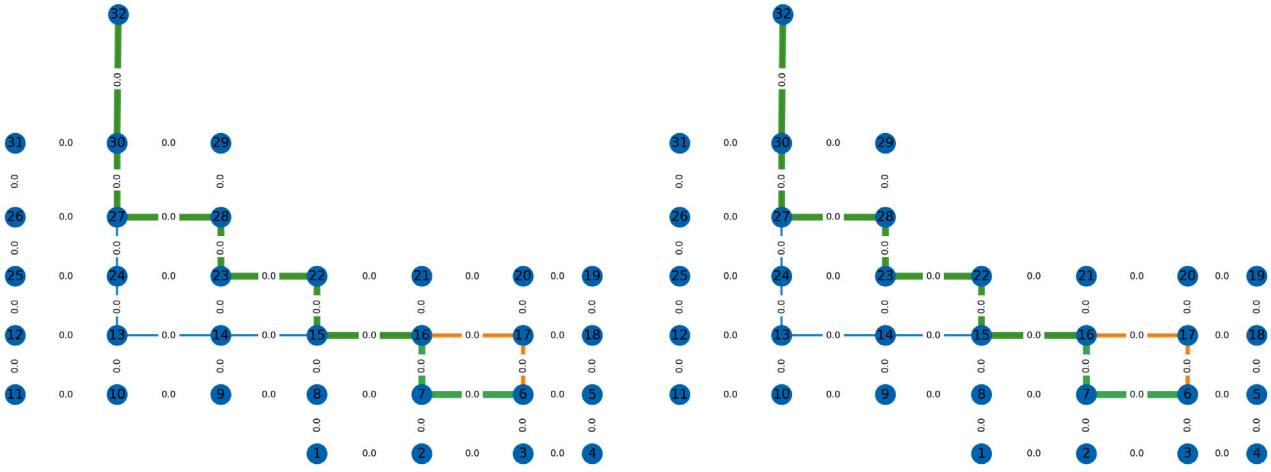

(c) 900 s (d) 1200 s

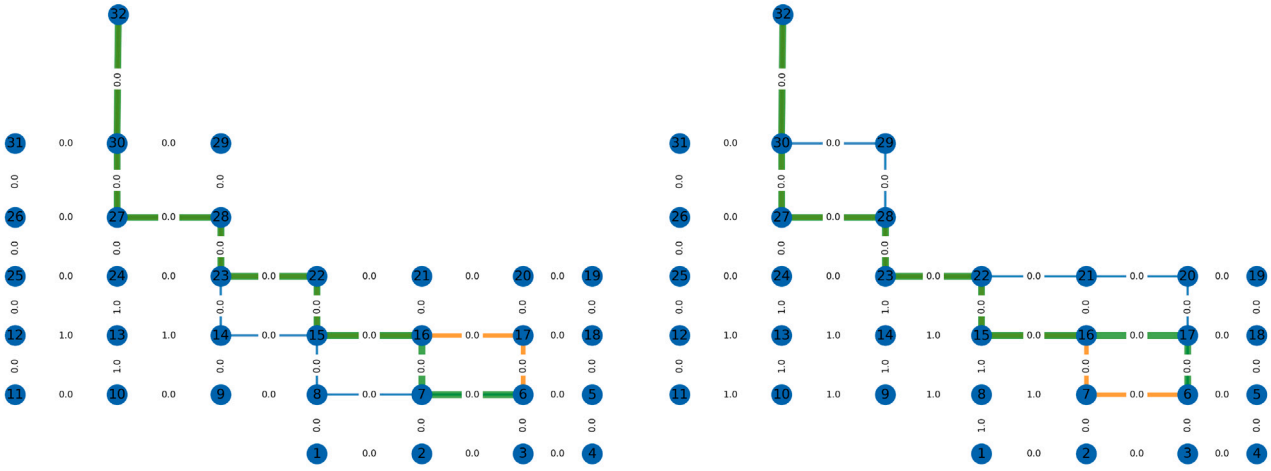

(e) 1500 s (f) 1800 s

Fig. 13. Optimum evacuation routes for different time points based on T_{wb} risk.

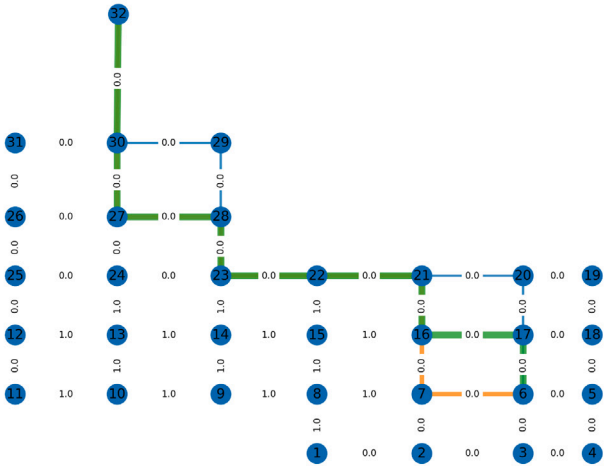

(g) 2100 s

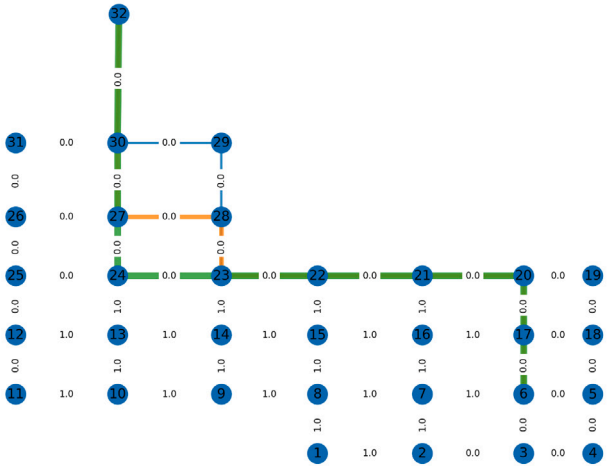

(h) 2400 s

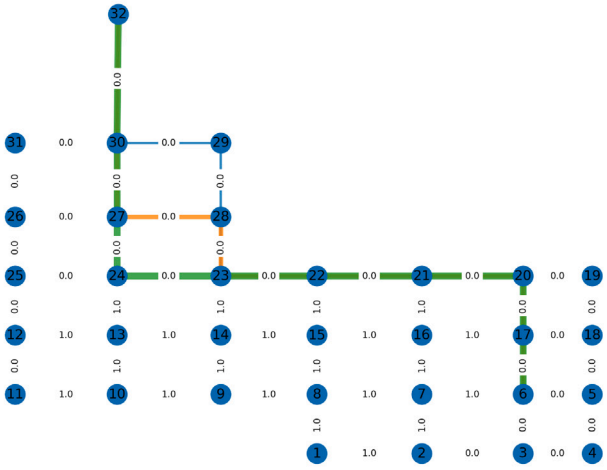

(i) 2700 s

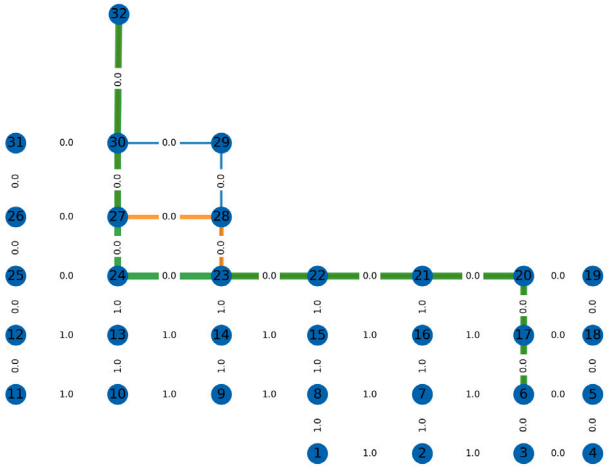

(j) 3000 s

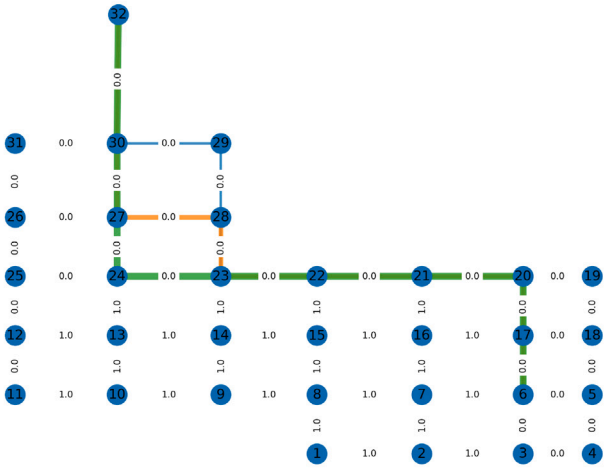

(k) 3300 s

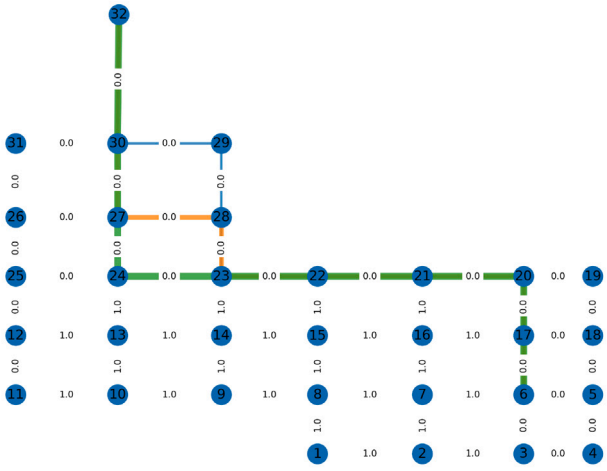

(l) 3600 s

Fig. 13. (*continued*).

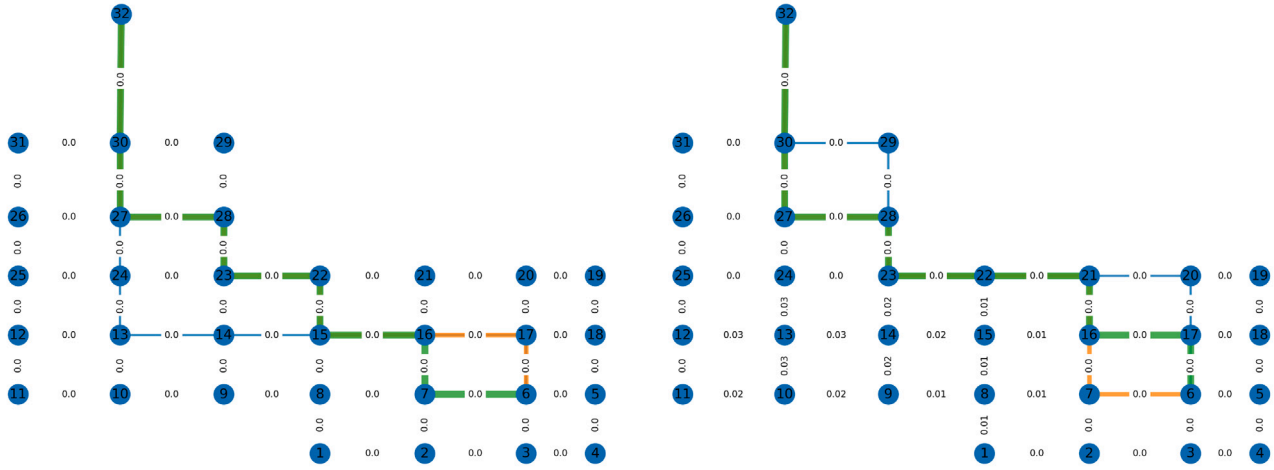

(a) 300 s

(b) 600 s

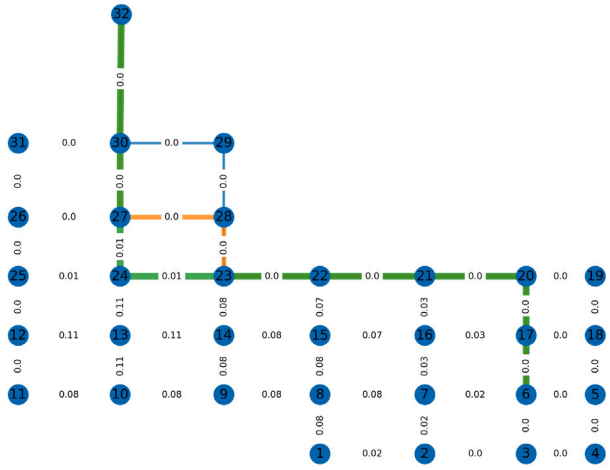

(c) 900 s

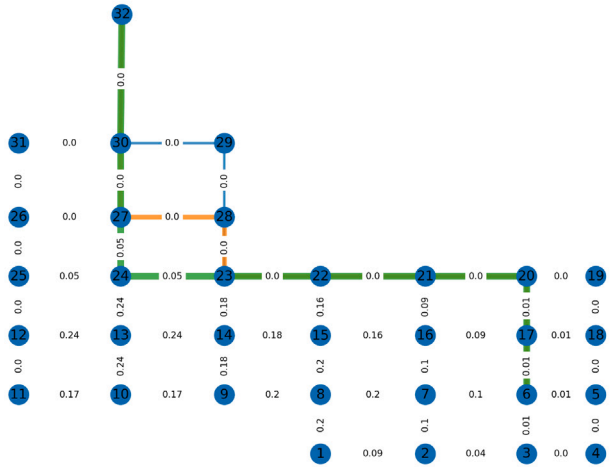

(d) 1200 s

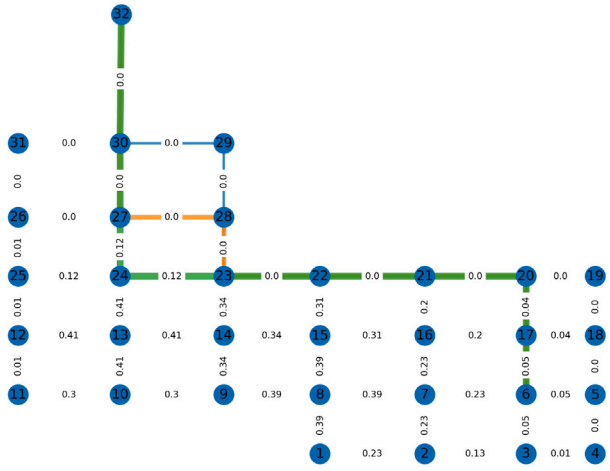

(e) 1500 s

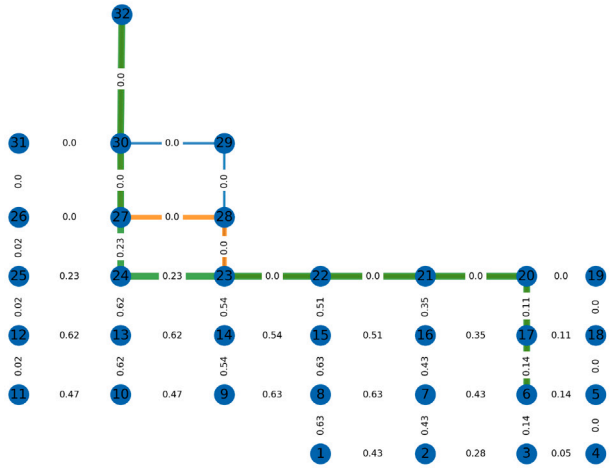

(f) 1800 s

Fig. 14. Optimum evacuation routes for different time points based on CO risk.

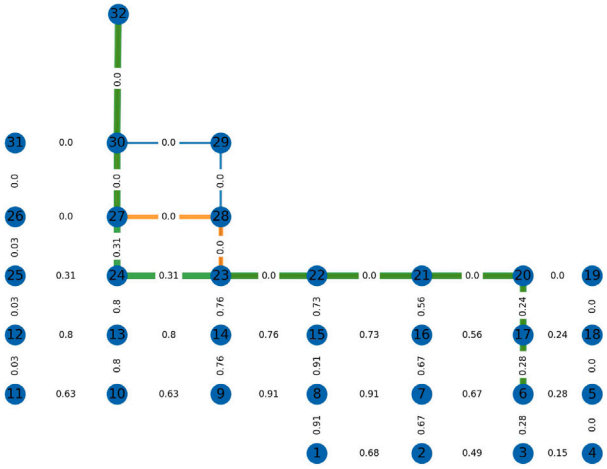

(g) 2100 s

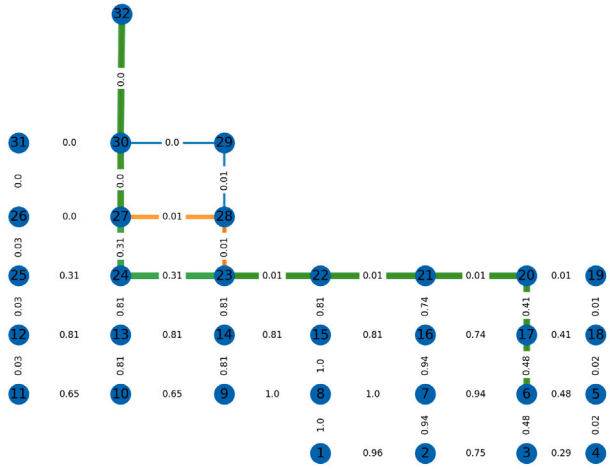

(h) 2400 s

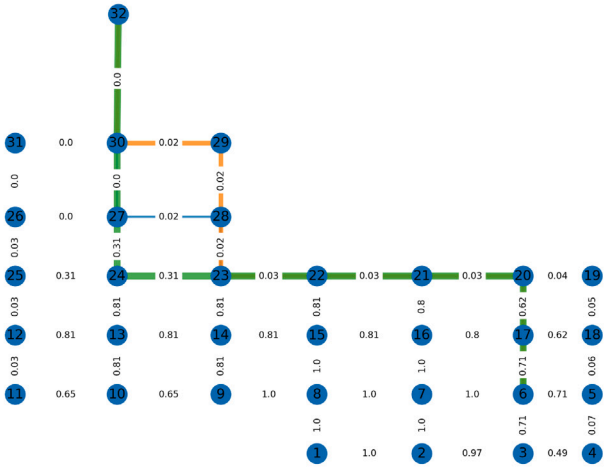

(i) 2700 s

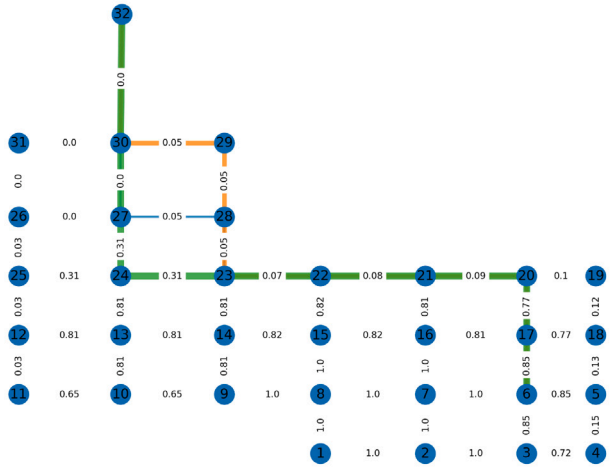

(j) 3000 s

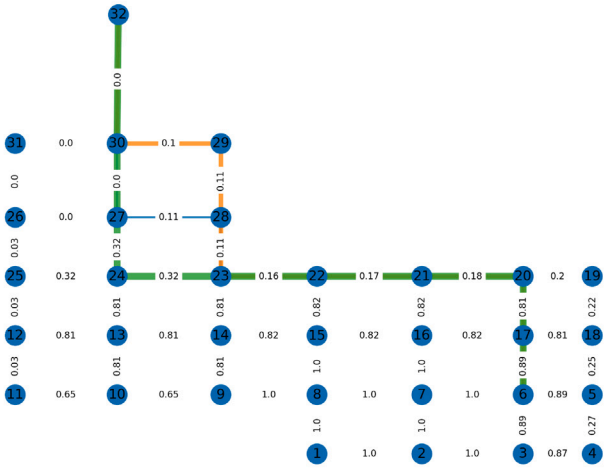

(k) 3300 s

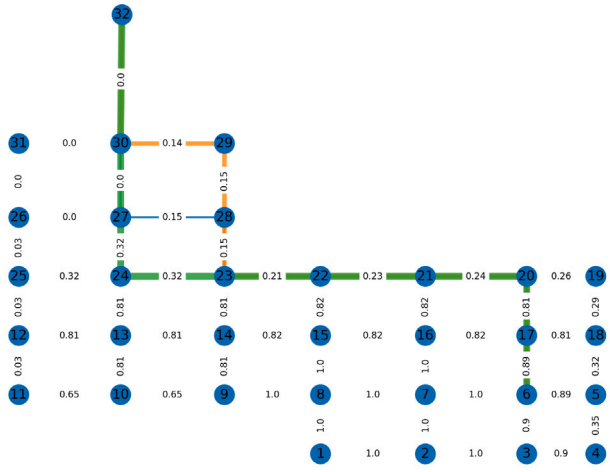

(l) 3600 s

Fig. 14. (*continued*).

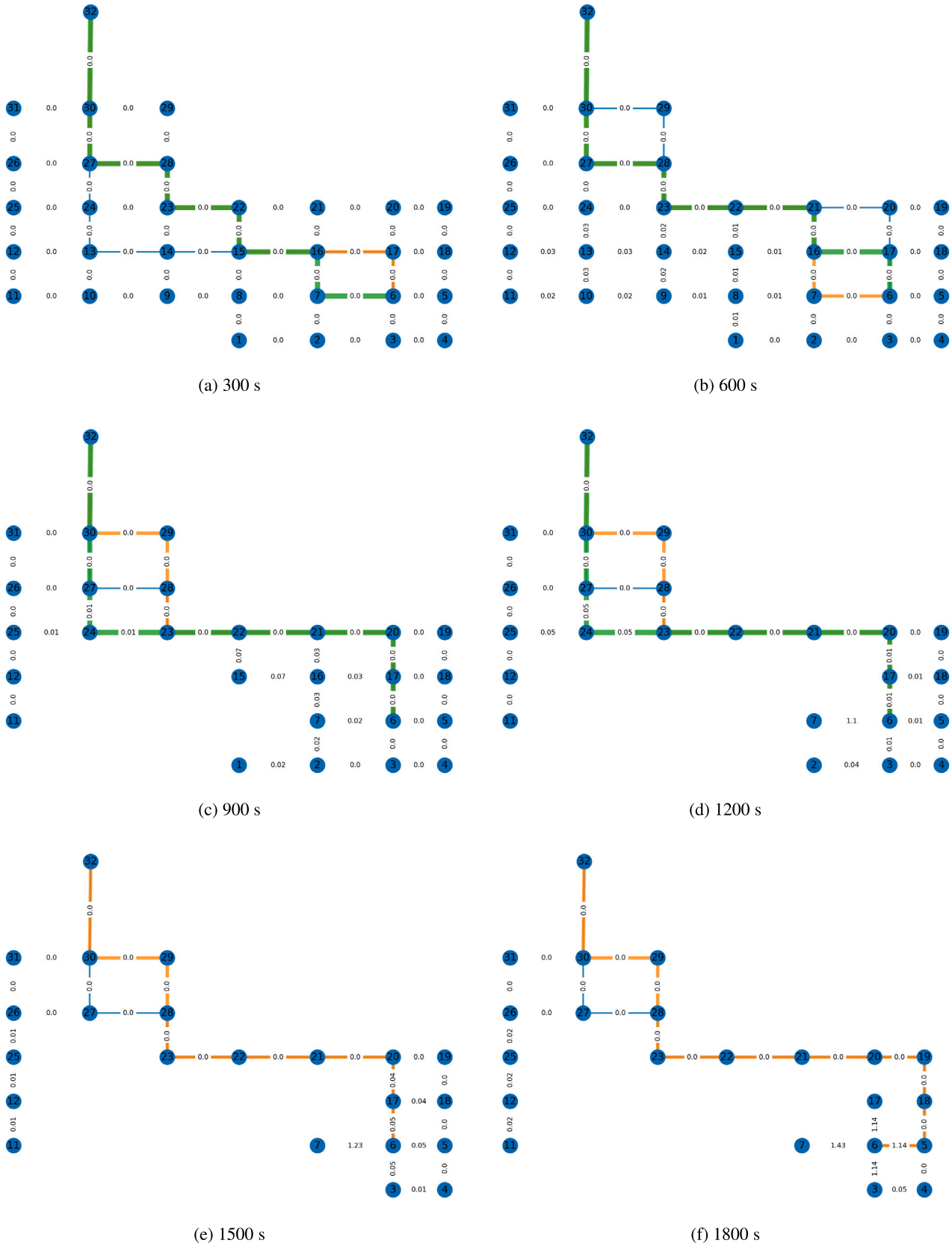

(a) 300 s (b) 600 s

(c) 900 s (d) 1200 s

(e) 1500 s (f) 1800 s

Fig. 15. Optimum evacuation routes for different time points based on the combined risk of the heat waves, the carbon monoxide fumes, the reduction of fresh air (O_2), and the visibility obstruction. Note that after 2400 s (40 min) there are no safe paths leading from the work area (node 6) to the exit (node 32).

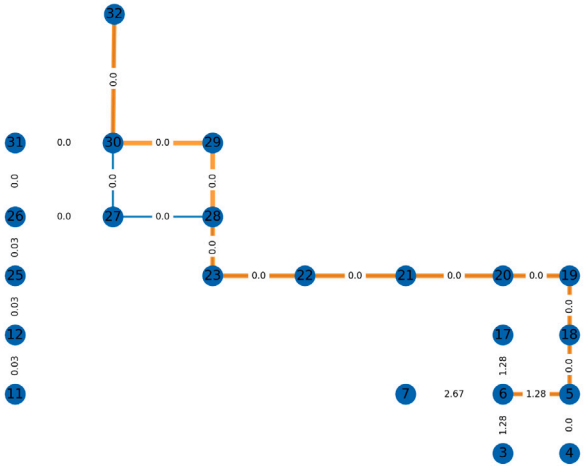

(g) 2100 s

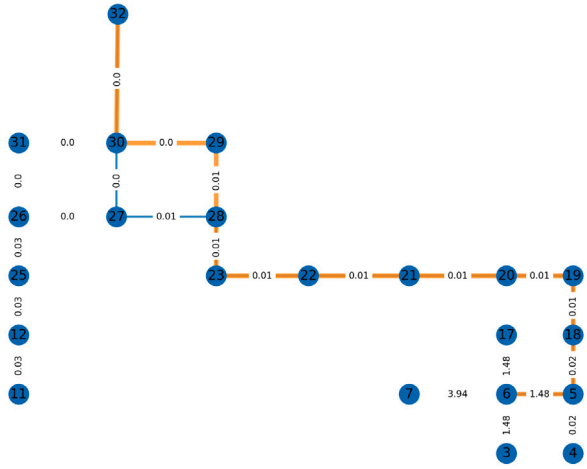

(h) 2400 s

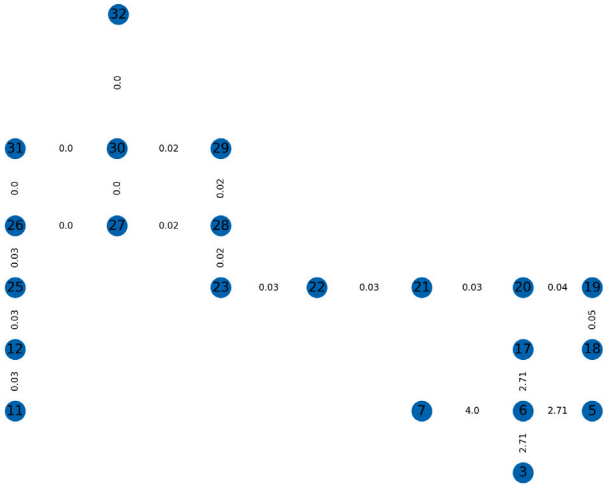

(i) 2700 s

(j) 3000 s

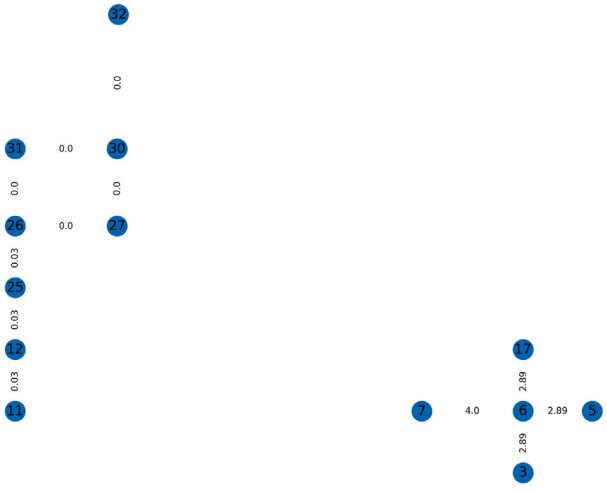

(k) 3300 s

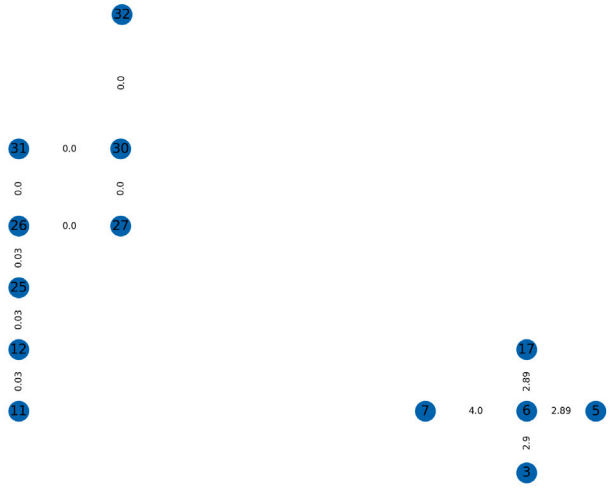

(l) 3600 s

Fig. 15. (*continued*).

Table 10
Cumulative risk and distance for optimum paths computed based on CO concentration.

Time (s)	Risk	Distance (m)
300	0.0, 0.0, 0.0	638.6, 638.6, 638.6
600	0.0, 0.0, 0.0	638.6, 638.6, 638.6
900	0.0, 0.0, 0.0	638.6, 638.6, 638.6
1200	0.0, 0.0, 0.1	638.6, 638.6, 638.6
1500	0.1, 0.1, 0.3	638.6, 638.6, 638.6
1800	0.2, 0.2, 0.7	638.6, 638.6, 638.6
2100	0.5, 0.5, 1.1	638.6, 638.6, 638.6
2400	0.9, 0.9, 1.5	638.6, 638.6, 638.6
2700	1.5, 1.5, 2.0	638.6, 638.6, 638.6
3000	2.0, 2.0, 2.5	638.6, 638.6, 638.6
3300	2.4, 2.5, 2.9	638.6, 638.6, 638.6
3600	2.7, 2.8, 3.0	638.6, 638.6, 638.6

is enclosed by the ventilation curtains. The ventilation curtains sufficiently keep the easternmost part of the eastern coal panel relatively safe for the remaining of the fire simulation, i.e., remaining 50 min. Thus, the optimum paths for that period remain unchangeable and head towards the return air pathways while outlining the ventilation curtains. Although the edges of the evacuation routes exhibit steadily increasing CO contamination, the maximum safety capacity is never exceeded. This means that evacuation is feasible even after 1 h after the fire starts when only the CO contamination risk is considered. Table 10 shows that all the viable evacuation routes have the shortest distance to the exit (i.e., 638.6 m). On the other hand, the cumulative risk of these routes steadily increases with the values exceeding 1.5 for the last 20 min. Table 11 shows that there are 32 additional shortest (i.e., total distance is 638.6 m) and safe paths for every time-point examined. However, the average cumulative risk of the 35 shortest paths starts increasing from 0.0 up to 5.8 after 10 min. Finally, Table 12 shows that there are 32,359 possible and safe paths (independently of total distance) for every time-point examined. The total distance of these paths can be as long as 1896.6 m, i.e., almost three times the distance of the shortest paths, while the cumulative risk raises up to more than 2.5 times the maximum cumulative risk of the shortest paths, i.e., 16.6 against 5.8.

Fig. 15 shows the output evacuation routes for the third scenario. Naturally, the combined fire-induced risks pose greater danger than the individual heat wave and CO contamination risks. The optimal evacuation routes computed for this scenario go through the vicinity of the fire up to only 5 min after the fire starts, while after 10 min the combined risk imposes slight detours to the optimal evacuation paths. After only 15 min the combined fire-induced risk has rendered the area west of the working location unsafe for evacuation (area that is enclosed by the ventilation curtains). Thus, the optimum paths for the remaining of the fire incident are restricted to the return air pathways and outline the ventilation curtains. Moreover, after 15 min of the fire emergency a portion of the mine has become critically unsafe (the nodes of the portion that are not illustrated in the maps). Additionally, there are only two shortest viable evacuation routes between the period of 25–45 min from the start of the fire (instead of the requested three), whereas there are no safe evacuation routes 45 min after the fire starts. Finally, it must be noted that after 30 min the evacuation routes are longer than the routes computed before that time-point due to the combined risks propagation. Also, even though the implemented FFA outputs these routes as viable, the first edge is unsafe (risk is higher than 1.0). This is related to assumption (d) as discussed in Section 4.3. As a result, the combined fire-induced risk indicates that the miners must decide on an evacuation plan at the latest 25 min after the fire has started. Table 13 shows that for the first 25 min all the viable evacuation routes have the shortest distance to the exit (i.e., 638.6 m) while the cumulative risks of these paths remain low. Table 14 shows that there are 32 additional shortest (i.e., total distance is 638.6 m) and safe paths only for the first 10 min of the fire emergency but the number of viable shortest paths significantly drops after that time-point. Between the period 25–40 min only two shortest paths are available, while between the period 30–40 min the shortest paths have an increased length of 707.4 m. Finally, Table 15 shows that there are 32,359 possible and safe paths (independently of total distance) only for the first 10 min of the fire emergency, but the number of viable paths significantly drops after that time-point. Between the period 30–40 min only 3 safe paths are available with total lengths between the range of 707.4–741.1 m. After 40 min there are no safe (shortest or not) paths. Although, the maximum cumulative risk for both the shortest and all possible paths does not exceed the value of 1.6, the combined fire-induced risk severely restricts the options for evacuation paths as well as the reaction time of the miners.

5. Discussion and conclusions

A fire emergency simulation is conducted with the VentFIRE™ tool of the VentSim™ DESIGN software for an underground mine. Based on the data collected by virtual sensors and a Ford-Fulkerson algorithm, we compute optimal evacuation routes for the miners during the emergency. Even though the VentFIRE™ software computes evacuation routes based on the impact of the highest risk, the user cannot define the safety criteria. Moreover, the evacuation routes depend only on the parameters that the software can simulate. On the other side, the proposed approach allows for defining the desired safety criteria, as well as for integrating data from multiple sources besides the VentFIRE™ simulation. This approach quantifies the emergency hazards based on the established safety and health regulations. Nevertheless, both the VentSim™ DESIGN software and the FFA should be used in combination with the context of any study case to obtain useful insights. Although, these approaches allow for modeling the dynamic progress of a fire event in an underground mine, there are no models that can accurately predict the progress and chemistry of a fire that starts in a certain way at a certain location of a mine.

Overall, the topology of the modeled mine and the applied ventilation system significantly reduce the speed at that the fire fumes spread towards the return air pathways (as is intended by the design of the ventilation system). However, the ventilation system directs the fire fumes towards the refuge chamber and reduces the time margin for the workers to seek shelter there. The airflow direction is defined by the ventilation system as well as the ventilation curtains and seals, are the primary causes of the observed behavior of the simulated fire fumes.

Based on the simulated sensors measurements, the miners have approximately 20–25 min to enter the refuge chamber and approximately 35–40 min to evacuate towards the exit through the ‘return air’ part of the mine. After 40 min (2700 s) the contaminated air starts to return through the return air pathways, which increases the risk of evacuation through the last safe pathways. Additionally, the miners need approximately 10–12 min (600–700 s) to evacuate from the working area to the exit towards the surface (a distance in the range of 600–700 m traversed with an average evacuation speed of 1 m/s). In combination with the data, this indicates that the most critical period of the evacuation is between 10 and 25 min (600 to 1800 s), i.e., between the first safety limit breaches occur after the fire starts (without considering the immediate vicinity of the fire) and the latest moment that the miners must start evacuating so that they can reach the exit before their last evacuation route becomes unsafe. This is the interval that the miners must decide on the escape plan to follow and act towards that speedily.

The simulated sensors were set to collect data for five different parameters: velocity of the airflow (m/s), carbon monoxide concentration (ppm), oxygen concentration (%), wet bulb temperature (°C), and visibility (m). Although the measurements of the latest four parameters exhibit significant changes during the simulation, the measurements

Table 11
Cumulative risk and distance for all shortest paths computed based on CO concentration.

Time (s)	No. of paths	Risk	Distance (m)
300	35	min: 0.0, max: 0.0, avg: 0.0	min: 638.6, max: 638.6, avg: 638.6
600	35	min: 0.0, max: 0.1, avg: 0.0	min: 638.6, max: 638.6, avg: 638.6
900	35	min: 0.0, max: 0.5, avg: 0.2	min: 638.6, max: 638.6, avg: 638.6
1200	35	min: 0.0, max: 1.2, avg: 0.6	min: 638.6, max: 638.6, avg: 638.6
1500	35	min: 0.1, max: 2.3, avg: 1.3	min: 638.6, max: 638.6, avg: 638.6
1800	35	min: 0.2, max: 3.7, avg: 2.2	min: 638.6, max: 638.6, avg: 638.6
2100	35	min: 0.5, max: 5.2, avg: 3.2	min: 638.6, max: 638.6, avg: 638.6
2400	35	min: 0.9, max: 5.7, avg: 3.8	min: 638.6, max: 638.6, avg: 638.6
2700	35	min: 1.5, max: 5.7, avg: 4.0	min: 638.6, max: 638.6, avg: 638.6
3000	35	min: 2.0, max: 5.7, avg: 4.1	min: 638.6, max: 638.6, avg: 638.6
3300	35	min: 2.4, max: 5.8, avg: 4.3	min: 638.6, max: 638.6, avg: 638.6
3600	35	min: 2.7, max: 5.8, avg: 4.4	min: 638.6, max: 638.6, avg: 638.6

Table 12
Cumulative risk and distance for all possible paths computed based on CO concentration.

Time (s)	No. of paths	Risk	Distance (m)
300	32 359	min: 0.0, max: 0.0, avg: 0.0	min: 638.6, max: 1896.6, avg: 1311.5
600	32 359	min: 0.0, max: 0.2, avg: 0.1	min: 638.6, max: 1896.6, avg: 1311.5
900	32 359	min: 0.0, max: 0.9, avg: 0.6	min: 638.6, max: 1896.6, avg: 1311.5
1200	32 359	min: 0.0, max: 2.3, avg: 1.5	min: 638.6, max: 1896.6, avg: 1311.5
1500	32 359	min: 0.1, max: 4.5, avg: 3.0	min: 638.6, max: 1896.6, avg: 1311.5
1800	32 359	min: 0.1, max: 7.6, avg: 5.0	min: 638.6, max: 1896.6, avg: 1311.5
2100	32 359	min: 0.3, max: 11.1, avg: 7.4	min: 638.6, max: 1896.6, avg: 1311.5
2400	32 359	min: 0.6, max: 13.2, avg: 8.8	min: 638.6, max: 1896.6, avg: 1311.5
2700	32 359	min: 1.0, max: 14.5, avg: 9.6	min: 638.6, max: 1896.6, avg: 1311.5
3000	32 359	min: 1.5, max: 15.4, avg: 10.2	min: 638.6, max: 1896.6, avg: 1311.5
3300	32 359	min: 2.3, max: 16.2, avg: 10.8	min: 638.6, max: 1896.6, avg: 1311.5
3600	32 359	min: 2.7, max: 16.6, avg: 11.1	min: 638.6, max: 1896.6, avg: 1311.5

Table 13
Cumulative risk and distance for optimum paths computed based on heat waves, CO, O_2, and visibility.

Time (s)	Risk	Distance (m)
300	0.0, 0.0, 0.0	638.6, 638.6, 638.6
600	0.0, 0.0, 0.0	638.6, 638.6, 638.6
900	0.0, 0.0, 0.0	638.6, 638.6, 638.6
1200	0.0, 0.0, 0.1	638.6, 638.6, 638.6
1500	0.1, 0.1	638.6, 638.6
1800	1.1, 1.1	707.4, 707.4
2100	1.3, 1.3	707.4, 707.4
2400	1.6, 1.6	707.4, 707.4
2700	No safe paths	No safe paths
3000	No safe paths	No safe paths
3300	No safe paths	No safe paths
3600	No safe paths	No safe paths

for airflow velocity remain constant in every location throughout the duration of the simulation. Therefore, these measurements are not used in further analysis with the FFA algorithm. However, the velocity data can provide validation for the ventilation model. Moreover, the area of the tunnels could be derived through the equation $Q = v \times A$, where the Q is the airflow quantity, v is the velocity of the air flow, and A is the cross-section area of the tunnel. This would allow for detecting significant changes in the shape of the tunnels around the mines, i.e., possible roof or rib collapses, which would block the miners escape. However, the VentSim™ DESIGN software does not provide tools to model roof/rib falls, and hence integrating this type of information is not attempted in the current study.

The implementation of the proposed approach provides a means to quantify the different fire-induced health and safety risks, based on the MSHA health and safety standards, and integrate in an FFA to compute the optimal escape routes. The algorithm was implemented for three different scenarios regarding the assumed presence of different fire-induced hazards or combinations of them: (a) heat waves, (b) CO fumes, and (c) combination of heat waves, CO fumes, lack of O_2, and reduced visibility. The outputs of the FFA for the examined scenarios highlight the validity of the paths as these paths change over time in such a way that the evacuation routes avoid the compromised pathways. Naturally, the first two scenarios that consider only one fire-induced risk factor allow for more evacuation options as well as for a longer reaction time. The results of the algorithm for the combined fire-induce risk factors indicate that the miners have significantly less options for evacuation paths as well as a much shorter reaction time to decide on an evacuation plan.

The current study identifies a gap in mine emergency decision-making practices in terms of flexible integration of the dynamic state of a mine ventilation system into emergency evacuation planning and real-time decision-making. In a mine emergency, drastic changes to ventilation-related components result to drastic changes to the safety of a pathway, and these cannot be fully modeled with the existing software. Although the proposed approach is an ongoing work, this study illustrates the validity of the results and the potential of such an approach. However, the following limitations must be noted:

- The original problem statement is simplistic and cannot extensively model real case studies, since it includes only one fire (the location of which is arbitrarily, and not deterministically, selected), one working face, and one exit.
- The distance between the working face and the exit is relatively short compared to real incidents.
- More sophisticated evacuation path planning algorithms are available that the one used in this study.
- A built-in VentSIM simulation model was considered for recreating the studied data from a fire simulation in an underground coal mine. For the sake of simplicity, the authors chose to only ensure that the fundamental MSHA requirement of the 0.3 m/s

Table 14
Cumulative risk and distance for all shortest paths computed based on heat waves, CO, O_2, and visibility.

Time (s)	No. of paths	Risk	Distance (m)
300	35	min: 0.0, max: 0.0, avg: 0.0	min: 638.6, max: 638.6, avg: 638.6
600	35	min: 0.0, max: 0.1, avg: 0.0	min: 638.6, max: 638.6, avg: 638.6
900	15	min: 0.0, max: 0.2, avg: 0.1	min: 638.6, max: 638.6, avg: 638.6
1200	3	min: 0.0, max: 0.1, avg: 0.1	min: 638.6, max: 638.6, avg: 638.6
1500	2	min: 0.1, max: 0.1, avg: 0.1	min: 638.6, max: 638.6, avg: 638.6
1800	2	min: 1.1, max: 1.1, avg: 1.1	min: 707.4, max: 707.4, avg: 707.4
2100	2	min: 1.3, max: 1.3, avg: 1.3	min: 707.4, max: 707.4, avg: 707.4
2400	2	min: 1.6, max: 1.6, avg: 1.6	min: 707.4, max: 707.4, avg: 707.4
2700	0	No safe paths	No safe paths
3000	0	No safe paths	No safe paths
3300	0	No safe paths	No safe paths
3600	0	No safe paths	No safe paths

Table 15
Cumulative risk and distance for all possible paths computed based on heat waves, CO, O_2, and visibility.

Time (s)	No. of paths	Risk	Distance (m)
300	32 359	min: 0.0, max: 0.0, avg: 0.0	min: 638.6, max: 1896.6, avg: 1311.5
600	32 359	min: 0.0, max: 0.2, avg: 0.1	min: 638.6, max: 1896.6, avg: 1311.5
900	470	min: 0.0, max: 0.2, avg: 0.1	min: 638.6, max: 1352.6, avg: 965.9
1200	60	min: 0.0, max: 0.1, avg: 0.1	min: 638.6, max: 1080.6, avg: 836.2
1500	18	min: 0.1, max: 0.1, avg: 0.1	min: 638.6, max: 944.6, avg: 775.0
1800	6	min: 1.1, max: 1.2, avg: 1.2	min: 707.4, max: 944.6, avg: 809.1
2100	3	min: 1.3, max: 1.3, avg: 1.3	min: 707.4, max: 808.6, avg: 741.1
2400	3	min: 1.6, max: 1.6, avg: 1.6	min: 707.4, max: 808.6, avg: 741.1
2700	0	No safe paths	No safe paths
3000	0	No safe paths	No safe paths
3300	0	No safe paths	No safe paths
3600	0	No safe paths	No safe paths

airflow speed in working areas is fulfilled. No further validation of the representative nature of this model or the applicability of the proposed method to other models and real-world scenarios has been conducted to date.
- The quantification of the fire-induced risks has not been rigorously validated against actual human health data. Although the individual hazards are quantified based on the MSHA standards (i.e., health limits), the combined risk may not correspond to a physically meaningful health index.

In the continuous efforts of the mining industry to improve safety and health of the mine workers, developing more sophisticated and smart evacuation techniques that use machine learning tools could play a crucial and life-saving role. Such tool could critically improve decision-making by providing mine-wide site-awareness, as well as alleviating the immense psychological distress miners undergo during an underground mine emergency. This study demonstrates the feasibility of a framework that can combine data from a hypothetical IoT (static or mobile), which collects real-time data, in an underground mine and graph theory to provide decision-making tools for self-evacuation. In mine emergencies, the miner is often aware only of his surrounding environment, whereas information about the state of the whole mine would be extremely valuable to a miner and improve the chances for safe and fast self-evacuation.

CRediT authorship contribution statement

Simon Lotero: Methodology, Software, Investigation, Writing – original draft, Visualization. **Vasilis Androulakis:** Conceptualization, Methodology, Software, Validation, Writing – review & editing. **Hassan Khaniani:** Conceptualization, Methodology, Writing – original draft preparation. **Mostafa Hassanalian:** Conceptualization, Writing – review & editing, Supervision, Project administration. **Sihua Shao:** Conceptualization, Writing – review & editing, Supervision, Project administration. **Pedram Roghanchi:** Conceptualization, Supervision, Project administration, Funding acquisition.

Declaration of competing interest

The authors declare that they have no known competing financial interests or personal relationships that could have appeared to influence the work reported in this paper.

Data availability

No data was used for the research described in the article.

Acknowledgments

This study was funded by the National Institute for Occupational Safety and Health (NIOSH) under the award #U60OH012351. The views, opinions, and recommendations expressed herein are solely those of the authors and do not necessarily reflect the views of NIOSH. Mentions of trade names, commercial products, or organizations does not imply endorsement by the authors nor the funding organization.

Appendix. VentSim™ Simulation Data

The simulation data of the five parameters of interest as recorded by all 32 sesors during 1 h of simulation can be seen in Tables A.1–A.5.

Table A.1
Airflow velocity simulation results in m/s as recorded by the 32 sensors during 1 h of simulation.

Time (s)	1	2	3	4	5	6	7	8	15	16	17	18	19	20	21	22	9	10	11	12	13	14	23	24	25	26	27	28	29	30	31	32
1	0.2	0.2	0.1	1.8	1.8	0.4	0.2	0.4	0.2	0.2	0.2	1.8	0.9	1.8	1.8	2.1	1.8	0.3	0.9	1.8	1.8	0.1	1.8	2.1	2.1	2.1	2.1	2.8	2.7	2.2	2.1	2.9
300	0.2	0.2	0.1	1.8	1.8	0.4	0.2	0.4	0.2	0.2	0.2	1.8	0.9	1.8	1.8	2.1	1.8	0.3	0.9	1.8	1.8	0.1	1.8	2.1	2.1	2.1	2.1	2.8	2.7	2.2	2.1	2.9
600	0.2	0.2	0.1	1.8	1.8	0.4	0.2	0.4	0.2	0.2	0.2	1.8	0.9	1.8	1.8	2.1	1.8	0.3	0.9	1.8	1.8	0.1	1.8	2.1	2.1	2.1	2.1	2.8	2.7	2.2	2.1	2.9
900	0.2	0.2	0.1	1.8	1.8	0.4	0.2	0.4	0.2	0.2	0.2	1.8	0.9	1.8	1.8	2.1	1.8	0.3	0.9	1.8	1.8	0.1	1.8	2.2	2.2	2.1	2.1	2.8	2.7	2.2	2.1	2.9
1200	0.2	0.2	0.1	1.8	1.8	0.4	0.2	0.4	0.2	0.2	0.2	1.8	0.9	1.8	1.8	2.1	1.8	0.3	0.9	1.8	1.9	0.1	1.8	2.2	2.2	2.1	2.1	2.8	2.7	2.2	2.1	2.9
1500	0.2	0.2	0.1	1.8	1.8	0.4	0.2	0.4	0.2	0.2	0.2	1.8	0.9	1.8	1.8	2.1	1.8	0.3	0.9	1.9	1.9	0.1	1.8	2.3	2.3	2.1	2.1	2.8	2.7	2.2	2.1	2.9
1800	0.2	0.2	0.1	1.8	1.8	0.4	0.2	0.4	0.2	0.2	0.2	1.8	0.9	1.8	1.8	2.1	1.8	0.3	0.9	1.9	1.9	0.1	1.8	2.4	2.3	2.1	2.1	2.8	2.7	2.2	2.1	2.9
2100	0.3	0.2	0.1	1.8	1.8	0.4	0.2	0.4	0.2	0.2	0.2	1.8	0.9	1.8	1.8	2.1	1.8	0.3	0.9	1.9	2.0	0.1	1.8	2.4	2.3	2.1	2.1	2.8	2.7	2.2	2.1	2.9
2400	0.3	0.2	0.1	1.8	1.8	0.4	0.2	0.4	0.2	0.2	0.2	1.8	0.9	1.8	1.8	2.1	1.8	0.3	0.9	1.9	2.0	0.1	1.8	2.4	2.3	2.1	2.1	2.8	2.7	2.2	2.1	2.9
2700	0.3	0.2	0.1	1.8	1.8	0.4	0.2	0.4	0.2	0.2	0.2	1.8	0.9	1.8	1.8	2.1	1.8	0.3	0.9	1.9	2.0	0.1	1.8	2.4	2.3	2.1	2.1	2.8	2.7	2.2	2.1	2.9
3000	0.3	0.2	0.1	1.8	1.8	0.4	0.2	0.4	0.2	0.2	0.2	1.8	0.9	1.8	1.8	2.1	1.8	0.3	0.9	1.9	2.0	0.1	1.8	2.4	2.3	2.1	2.1	2.8	2.7	2.2	2.1	2.9
3300	0.3	0.2	0.1	1.8	1.8	0.4	0.2	0.4	0.2	0.2	0.2	1.8	0.9	1.8	1.8	2.1	1.8	0.3	0.9	1.9	2.0	0.1	1.8	2.4	2.3	2.1	2.1	2.8	2.7	2.2	2.1	2.9
3600	0.3	0.2	0.1	1.8	1.8	0.4	0.2	0.4	0.2	0.2	0.2	1.8	0.9	1.8	1.8	2.1	1.8	0.3	0.9	1.9	2.0	0.1	1.8	2.4	2.3	2.1	2.1	2.8	2.7	2.2	2.1	2.9

Table A.2
Temperature wet bulb results in °C as recorded by the 32 sensors during 1 h of simulation.

Time (s)	1	2	3	4	5	6	7	8	15	16	17	18	19	20	21	22	9	10	11	12	13	14	23	24	25	26	27	28	29	30	31	32
1	21.2	21.2	21.0	21.5	21.5	21.1	21.2	21.3	21.4	21.3	21.1	21.5	21.5	21.5	21.5	21.4	20.8	21.4	21.3	21.3	21.3	21.4	21.0	21.2	21.3	21.2	21.2	21.2	21.2	21.2	21.2	21.2
300	21.3	21.2	21.0	21.5	21.5	21.1	21.2	21.1	21.1	21.2	21.1	21.5	21.5	21.5	21.5	21.4	20.8	21.1	21.1	21.1	21.2	21.1	21.1	21.1	21.1	21.1	21.1	21.3	21.2	21.1	21.1	21.1
600	21.0	21.1	21.0	21.5	21.5	21.1	21.0	21.2	21.3	21.1	21.1	21.5	21.5	21.4	21.4	21.4	20.8	21.5	21.0	21.1	22.1	21.4	21.0	21.1	21.1	21.1	21.1	21.2	21.2	21.1	21.1	21.1
900	21.2	21.0	21.1	21.5	21.5	21.0	21.2	22.0	22.1	21.3	21.0	21.5	21.5	21.4	21.4	21.4	20.8	22.6	21.1	21.1	23.9	22.5	21.0	21.4	21.1	21.1	21.1	21.2	21.2	21.1	21.1	21.1
1200	22.0	21.3	20.9	21.5	21.5	21.0	22.1	23.6	23.5	22.1	20.9	21.5	21.5	21.4	21.4	21.4	20.8	24.1	21.0	21.1	26.2	24.1	21.0	22.3	21.1	21.1	21.1	21.2	21.2	21.1	21.1	21.1
1500	23.4	22.3	20.9	21.5	21.5	21.4	23.6	25.5	25.1	23.3	21.2	21.5	21.5	21.5	21.4	21.4	20.8	25.7	21.1	21.1	28.3	25.9	21.0	23.6	21.2	21.1	21.1	21.2	21.2	21.1	21.1	21.1
1800	24.9	23.5	21.3	21.5	21.5	22.3	25.1	27.4	26.8	24.7	22.0	21.5	21.5	21.5	21.4	21.4	20.8	27.2	21.2	21.3	30.4	27.7	21.0	25.2	21.4	21.1	21.1	21.2	21.2	21.1	21.1	21.1
2100	26.4	24.7	22.1	21.5	21.5	23.4	26.7	29.4	28.6	26.3	23.1	21.5	21.5	21.4	21.4	21.4	20.9	28.6	21.4	21.5	31.9	29.5	21.1	26.3	21.6	21.1	21.1	21.2	21.2	21.1	21.1	21.1
2400	27.8	25.9	22.9	21.6	21.6	24.4	28.1	30.3	29.2	27.4	24.0	21.5	21.5	21.4	21.4	21.4	20.9	28.9	21.4	21.5	32.2	29.9	21.1	26.5	21.6	21.1	21.1	21.2	21.2	21.1	21.1	21.1
2700	28.4	26.9	23.6	21.9	21.8	25.4	28.6	30.5	29.3	27.8	25.0	21.8	21.7	21.6	21.6	21.5	20.9	29.0	21.5	21.5	32.4	30.0	21.1	26.6	21.6	21.1	21.1	21.3	21.3	21.1	21.1	21.1
3000	28.5	27.2	24.3	22.5	22.4	25.9	28.8	30.7	29.4	28.0	25.6	22.2	22.1	22.0	21.9	21.8	20.9	29.2	21.5	21.5	32.6	30.2	21.3	26.7	21.6	21.1	21.1	21.5	21.5	21.1	21.1	21.1
3300	28.6	27.3	24.7	22.7	22.7	26.1	28.9	30.8	29.6	28.1	25.8	22.6	22.5	22.4	22.3	22.2	20.9	29.3	21.5	21.6	32.7	30.3	21.4	26.9	21.6	21.1	21.1	21.8	21.7	21.1	21.1	21.1
3600	28.7	27.4	24.8	22.8	22.7	26.2	29.0	30.9	29.6	28.1	25.9	22.6	22.5	22.4	22.4	22.3	20.9	29.4	21.5	21.6	32.8	30.4	21.5	26.9	21.7	21.1	21.1	21.8	21.8	21.1	21.1	21.1

Table A.3
Carbon monoxide concentration results in ppm as recorded by the 32 sensors during 1 h of simulation.

Time (s)	1	2	3	4	5	6	7	8	15	16	17	18	19	20	21	22	9	10	11	12	13	14	23	24	25	26	27	28	29	30	31	32
1	0.0	0.0	0.0	0.0	0.0	0.0	0.0	0.0	0.0	0.0	0.0	0.0	0.0	0.0	0.0	0.0	0.0	0.0	0.0	0.0	0.0	0.0	0.0	0.0	0.0	0.0	0.0	0.0	0.0	0.0	0.0	0.0
300	0.0	0.0	0.0	0.0	0.0	0.0	0.0	0.1	0.5	0.0	0.0	0.0	0.0	0.0	0.0	0.0	0.0	3.6	0.0	0.0	8.3	1.3	0.0	0.0	0.0	0.0	0.0	0.0	0.0	0.0	0.0	0.0
600	0.9	0.0	0.0	0.0	0.0	0.0	1.9	31.4	35.2	6.6	0.0	0.0	0.0	0.0	0.0	0.0	0.0	61.2	0.0	0.0	89.5	46.0	0.0	1.6	0.0	0.0	0.0	0.0	0.0	0.0	0.0	0.0
900	51.9	10.3	0.0	0.0	0.0	0.6	60.0	192.7	166.8	65.3	0.7	0.0	0.0	0.0	0.0	0.0	0.2	202.4	0.0	0.0	282.5	194.3	0.0	33.6	0.0	0.0	0.0	0.0	0.0	0.0	0.0	0.0
1200	242.3	103.7	1.2	0.0	0.0	24.6	252.3	509.4	419.8	223.1	16.4	0.0	0.0	0.0	0.0	0.0	1.7	442.9	1.1	2.1	602.5	467.5	0.3	134.9	2.7	0.0	0.0	0.1	0.1	0.0	0.0	0.0
1500	589.9	333.1	28.6	0.0	0.0	132.2	597.0	986.4	798.9	503.6	99.1	0.0	0.0	0.0	0.0	0.0	5.1	778.4	12.4	15.7	1041.1	864.7	1.4	316.7	17.3	0.0	0.0	0.5	0.5	0.0	0.0	0.0
1800	1094.6	716.6	139.8	0.4	0.2	361.7	1091.0	1602.0	1295.6	907.2	290.7	0.1	0.0	0.0	0.0	0.0	10.5	1198.6	37.4	43.1	1595.7	1378.1	3.6	585.4	45.9	0.0	0.0	1.4	1.3	0.0	0.0	0.0
2100	1736.9	1246.1	374.2	10.6	7.2	727.7	1719.8	2343.3	1874.8	1431.1	610.1	4.7	2.7	2.0	1.4	0.9	17.7	1613.8	72.1	76.0	2044.2	1940.9	7.4	792.7	77.3	0.0	0.0	3.3	2.9	0.0	0.0	0.0
2400	2464.9	1911.7	747.2	57.8	45.9	1224.9	2402.8	2723.2	2065.3	1901.9	1055.1	36.0	26.6	21.8	18.5	14.8	26.5	1677.3	81.2	81.3	2068.2	2067.1	17.2	799.5	81.4	0.0	0.0	13.2	11.1	0.0	0.0	0.0
2700	2715.9	2478.5	1255.4	172.4	146.7	1820.1	2605.5	2747.5	2084.7	2055.4	1594.7	123.8	101.4	88.2	79.2	68.8	33.8	1676.8	82.2	82.3	2069.7	2069.2	43.9	802.8	82.4	0.0	0.0	50.4	44.0	0.0	0.0	0.0
3000	2731.2	2625.9	1848.4	379.1	335.5	2187.0	2622.5	2751.4	2089.1	2083.2	1982.6	295.2	255.0	229.2	211.9	191.3	35.8	1676.1	83.1	83.3	2070.9	2070.5	97.7	805.9	83.4	0.0	0.0	135.5	122.2	0.0	0.0	0.0
3300	2734.6	2663.2	2219.9	693.3	628.8	2278.1	2627.1	2753.1	2091.0	2089.2	2068.2	567.6	506.8	465.0	437.8	404.4	38.1	1676.1	84.1	84.3	2072.6	2072.0	188.7	809.0	84.3	0.0	0.0	286.1	263.5	0.0	0.0	0.0
3600	2735.4	2671.4	2301.2	889.6	814.8	2291.2	2628.1	2754.1	2092.0	2090.3	2082.1	740.9	669.6	617.8	585.2	545.0	39.9	1675.9	84.6	84.8	2073.5	2072.9	248.9	810.4	84.8	0.0	0.0	386.2	358.7	0.0	0.0	0.0

Table A.4
Oxygen concentration results in % as recorded by the 32 sensors during 1 h of simulation.

Time (s)	1	2	3	4	5	6	7	8	15	16	17	18	19	20	21	22	9	10	11	12	13	14	23	24	25	26	27	28	29	30	31	32
1	21.0	21.0	21.0	21.0	21.0	21.0	21.0	21.0	21.0	21.0	21.0	21.0	21.0	21.0	21.0	21.0	21.0	21.0	21.0	21.0	21.0	21.0	21.0	21.0	21.0	21.0	21.0	21.0	21.0	21.0	21.0	21.0
300	21.0	21.0	21.0	21.0	21.0	21.0	21.0	21.0	21.0	21.0	21.0	21.0	21.0	21.0	21.0	21.0	21.0	21.0	21.0	21.0	21.0	21.0	21.0	21.0	21.0	21.0	21.0	21.0	21.0	21.0	21.0	21.0
600	21.0	21.0	21.0	21.0	21.0	21.0	21.0	20.9	20.9	21.0	21.0	21.0	21.0	21.0	21.0	21.0	21.0	20.9	21.0	21.0	20.9	20.9	21.0	21.0	21.0	21.0	21.0	21.0	21.0	21.0	21.0	21.0
900	20.9	21.0	21.0	21.0	21.0	21.0	20.9	20.8	20.9	20.9	21.0	21.0	21.0	21.0	21.0	21.0	21.0	20.8	21.0	21.0	20.8	20.8	21.0	20.9	21.0	21.0	21.0	21.0	21.0	21.0	21.0	21.0
1200	20.8	20.9	21.0	21.0	21.0	20.9	20.8	20.6	20.7	20.8	21.0	21.0	21.0	21.0	21.0	21.0	21.0	20.7	21.0	21.0	20.6	20.7	21.0	20.9	21.0	21.0	21.0	21.0	21.0	21.0	21.0	21.0
1500	20.6	20.8	20.9	21.0	21.0	20.9	20.6	20.3	20.5	20.6	20.9	21.0	21.0	21.0	21.0	21.0	21.0	20.5	21.0	21.0	20.3	20.4	21.0	20.8	21.0	21.0	21.0	21.0	21.0	21.0	21.0	21.0
1800	20.3	20.5	20.9	21.0	21.0	20.7	20.3	20.0	20.1	20.4	20.8	21.0	21.0	21.0	21.0	21.0	21.0	20.2	20.9	20.9	20.0	20.1	21.0	20.6	20.9	21.0	21.0	21.0	21.0	21.0	21.0	21.0
2100	19.9	20.2	20.7	21.0	21.0	20.5	19.9	19.5	19.8	20.1	20.6	21.0	21.0	21.0	21.0	21.0	21.0	19.9	20.9	20.9	19.7	19.7	21.0	20.5	20.9	21.0	21.0	21.0	21.0	21.0	21.0	21.0
2400	19.4	19.8	20.5	20.9	20.9	20.2	19.5	19.3	19.7	19.8	20.3	20.9	20.9	20.9	21.0	21.0	20.9	19.9	20.9	20.9	19.7	19.7	21.0	20.5	20.9	21.0	21.0	21.0	21.0	21.0	21.0	21.0
2700	19.3	19.4	20.2	20.9	20.9	19.8	19.3	19.2	19.7	19.7	20.0	20.9	20.9	20.9	20.9	20.9	20.9	19.9	20.9	20.9	19.7	19.7	20.9	20.5	20.9	21.0	21.0	20.9	20.9	21.0	21.0	21.0
3000	19.2	19.3	19.8	20.7	20.8	19.6	19.3	19.2	19.7	19.7	19.7	20.8	20.8	20.8	20.8	20.8	20.9	19.9	20.9	20.9	19.7	19.7	20.9	20.5	20.9	21.0	21.0	20.9	20.9	21.0	21.0	21.0
3300	19.2	19.3	19.6	20.5	20.6	19.5	19.3	19.2	19.6	19.7	19.7	20.6	20.6	20.7	20.7	20.7	20.9	19.9	20.9	20.9	19.7	19.7	20.8	20.5	20.9	21.0	21.0	20.8	20.8	21.0	21.0	21.0
3600	19.2	19.3	19.5	20.4	20.4	19.5	19.3	19.2	19.6	19.6	19.7	20.5	20.5	20.6	20.6	20.6	20.9	19.9	20.9	20.9	19.7	19.7	20.8	20.5	20.9	21.0	21.0	20.7	20.7	21.0	21.0	21.0

Table A.5
Visibility results in m (obstructed by smoke) as recorded by the 32 sensors during 1 h of simulation.

Time (s)	1	2	3	4	5	6	7	8	15	16	17	18	19	20	21	22	9	10	11	12	13	14	23	24	25	26	27	28	29	30	31	32
1	25.0	25.0	25.0	25.0	25.0	25.0	25.0	25.0	25.0	25.0	25.0	25.0	25.0	25.0	25.0	25.0	25.0	25.0	25.0	25.0	25.0	25.0	25.0	25.0	25.0	25.0	25.0	25.0	25.0	25.0	25.0	25.0
300	25.0	25.0	25.0	25.0	25.0	25.0	25.0	25.0	25.0	25.0	25.0	25.0	25.0	25.0	25.0	25.0	25.0	25.0	25.0	25.0	25.0	25.0	25.0	25.0	25.0	25.0	25.0	25.0	25.0	25.0	25.0	25.0
600	25.0	25.0	25.0	25.0	25.0	25.0	25.0	25.0	25.0	25.0	25.0	25.0	25.0	25.0	25.0	25.0	25.0	25.0	25.0	25.0	24.9	25.0	25.0	25.0	25.0	25.0	25.0	25.0	25.0	25.0	25.0	25.0
900	25.0	25.0	25.0	25.0	25.0	25.0	25.0	20.2	20.8	25.0	25.0	25.0	25.0	25.0	25.0	25.0	25.0	13.9	25.0	25.0	9.0	19.9	25.0	25.0	25.0	25.0	25.0	25.0	25.0	25.0	25.0	25.0
1200	17.1	24.9	25.0	25.0	25.0	25.0	16.6	4.0	5.0	14.5	25.0	25.0	25.0	25.0	25.0	25.0	25.0	3.5	25.0	25.0	2.4	4.6	25.0	19.2	25.0	25.0	25.0	25.0	25.0	25.0	25.0	25.0
1500	3.2	8.9	25.0	25.0	25.0	23.7	3.2	1.4	1.7	3.5	24.2	25.0	25.0	25.0	25.0	25.0	25.0	1.5	25.0	25.0	1.1	1.6	25.0	5.2	25.0	25.0	25.0	25.0	25.0	25.0	25.0	25.0
1800	1.2	2.2	24.5	25.0	25.0	7.3	1.2	0.7	0.9	1.4	8.1	25.0	25.0	25.0	25.0	25.0	25.0	0.8	25.0	24.9	0.6	0.8	25.0	2.1	24.7	25.0	25.0	25.0	25.0	25.0	25.0	25.0
2100	0.6	1.0	8.7	25.0	25.0	2.2	0.6	0.4	0.5	0.7	2.4	25.0	25.0	25.0	25.0	25.0	25.0	0.5	18.0	15.4	0.4	0.5	25.0	1.1	14.4	25.0	25.0	25.0	25.0	25.0	25.0	25.0
2400	0.4	0.5	2.5	25.0	25.0	1.0	0.4	0.3	0.3	0.5	1.1	25.0	25.0	25.0	25.0	25.0	25.0	0.4	8.8	8.2	0.3	0.3	25.0	0.8	8.0	25.0	25.0	25.0	25.0	25.0	25.0	25.0
2700	0.3	0.3	1.1	12.9	16.0	0.6	0.3	0.2	0.3	0.3	0.6	18.7	21.6	22.9	23.8	24.5	23.1	0.4	7.6	7.6	0.3	0.3	24.9	0.8	7.6	25.0	25.0	25.0	25.0	25.0	25.0	25.0
3000	0.2	0.3	0.6	4.0	4.7	0.4	0.2	0.2	0.3	0.3	0.4	5.6	7.1	8.1	9.1	10.5	18.2	0.4	7.5	7.5	0.3	0.3	15.4	0.8	7.5	25.0	25.0	14.1	16.0	25.0	25.0	25.0
3300	0.2	0.2	0.4	1.7	2.0	0.3	0.2	0.2	0.3	0.3	0.3	2.2	2.6	2.9	3.2	3.5	17.2	0.4	7.4	7.4	0.3	0.3	6.7	0.8	7.4	25.0	25.0	4.9	5.5	25.0	25.0	25.0
3600	0.2	0.2	0.3	0.9	1.0	0.3	0.2	0.2	0.3	0.3	0.3	1.1	1.3	1.4	1.5	1.6	16.2	0.4	7.3	7.3	0.3	0.3	3.4	0.8	7.3	25.0	25.0	2.3	2.5	25.0	25.0	25.0

References

Adjiski, V., Mirakovski, D., Despodov, Z., Mijalkovski, S., 2015. Simulation and optimization of evacuation routes in case of fire in underground mines. J. Sustain. Min. 14 (3), 133–143.

Aminossadati, S.M., Hooman, K., 2014. Numerical Simulation of Ventilation Air Flow in Underground Mine Workings. Report.

Belle, B., 2013. Real-time air velocity monitoring in mines-a quintessential design parameter for managing major mine health and safety hazards.

Brake, D., 2013. Fire modelling in underground mines using Ventsim Visual VentFIRE Software. In: Proceedings of the Australian Mine Ventilation Conference, Adelaide, SA, Australia. pp. 1–3.

Brnich, M., Kowalski-Trakofler, K.M., Brune, J., 2010. Underground coal mine disasters 1900–2010: Events, responses, and a look to the future. In: Extracting the Science: a Century of Mining Research. Littleton, CO: Society of Mining, Metallurgy, and Exploration, pp. 363–372.

Burkard, R.E., Dlaska, K., Klinz, B., 1993. The quickest flow problem. Z. Oper. Res. 37 (1), 31–58.

Chalmet, L.G., Francis, R.L., Saunders, P.B., 1982. Network models for building evacuation. Manage. Sci. 28 (1), 86–105.

Chen, J., Chen, H., Fu, S., 2003. Numerical study of reversal flow in tunnel fires. Int. J. Eng. Perform.-Based Fire Codes 5, 194–198.

Conti, R.S., 2001. Responders to underground mine fires. In: Proceedings of the 32nd Annual Conference of the Institute on Mining Health, Safety and Research. pp. 111–121.

Conti, R.S., Chasko, L.L., Wiehagen, W.J., Lazzara, C.P., 2005. Fire Response Preparedness for Underground Mines. DHHS IC 9481. US Department of Health and Human Services, Public Health Service, Centers for Disease Control and Prevention, National Institute for Occupational Safety and Health, Pittsburgh Research Laboratory.

Coutinho-Rodrigues, J., Tralhão, L., Alçada-Almeida, L., 2012. Solving a location-routing problem with a multiobjective approach: the design of urban evacuation plans. J. Transp. Geogr. 22, 206–218.

Cui, J., An, S., Zhao, M., 2014. A generalized minimum cost flow model for multiple emergency flow routing. Math. Probl. Eng. 2014, http://dx.doi.org/10.1155/2014/832053.

Deng, K., Hu, L., Zhang, Q., Zhang, D., Chen, J., Fan, W., 2022. Emergency evacuation scheme of cruise ship under fire situation based on multi-source multi-sink maximum flow model. In: 2022 37th Youth Academic Annual Conference of Chinese Association of Automation. YAC, IEEE, pp. 728–733.

Düzgün, H.S., Leveson, N., 2018. Analysis of soma mine disaster using causal analysis based on systems theory (CAST). Saf. Sci. 110, 37–57.

Ford, L.R., Fulkerson, D.R., 1956. Maximal flow through a network. Canad. J. Math. 8, 399–404.

Ford, L.R., Fulkerson, D.R., 1963. Flows in Networks. Princeton University Press, http://dx.doi.org/10.1515/9781400875184.

Goh, J., 2021. A literature review of medical support in cave rescue and confined space medicine - Implications in urban underground space development. In: IOP Conference Series: Earth and Environmental Science. Vol. 703, IOP Publishing Ltd, pp. 12–42. http://dx.doi.org/10.1088/1755-1315/703/1/012042.

Goldberg, A.V., Tarjan, R.E., 1988. A new approach to the maximum-flow problem. J. Assoc. Comput. Mach. 35 (4), 921–940.

Hamacher, H.W., Tjandra, S.A., 2001. Mathematical modelling of evacuation problems: A state of art. In: Proceedings of Pedestrian and Evacuation Dynamics. Berlin, pp. 59–74.

Howden Group, 2020. VentSim DESIGN™ user guide. URL: https://ventsim.com/files/VentsimManual.pdf.

IMG PAN, 2023. VentGraph – software for mine ventilation engineers and experts. URL: https://imgpan.pl/en/oferta/ventgraph/.

Jin, J.G., Shen, Y., Hu, H., Fan, Y., Yu, M., 2021. Optimizing underground shelter location and mass pedestrian evacuation in urban community areas: A case study of Shanghai. Transp. Res. A 149, 124–138.

Kevin, G.S., Linda, F.Z., 2011. The Danger of Oxygen Deficiency in Underground Coal Mines. Report.

Kowalski-Trakofler, K., Alexander, D., Brnich, M., McWilliams, L., Podlesny, A., Lenart, P., 2009. Underground coal mining disasters and fatalities–United States, 1900–2006. MMWR: Morb. Mortal. Wkly Rep. 57 (51), 1379–1383.

Kriebel, D., Checkoway, H., Pearce, N., 2007. Exposure and dose modelling in occupational epidemiology. Occup. Environ. Med. 64 (7), 492–498.

Lavrov, M., 2020. When Augmenting Paths Fail Proving the Residual Graph Theorem Max-Flow Algorithms. Report.

Li, W., Wang, G.-G., Gandomi, A.H., 2021. A survey of learning-based intelligent optimization algorithms. Arch. Comput. Methods Eng. 28, 3781–3799.

Lin, P., Lo, S.M., Huang, H.-C., Yuen, K., 2008. On the use of multi-stage time-varying quickest time approach for optimization of evacuation planning. Fire Saf. J. 43 (4), 282–290.

Liu, L., Jin, H., Liu, Y., Zhang, X., 2022. Intelligent evacuation route planning algorithm based on maximum flow. Int. J. Environ. Res. Public Health 19 (13), 7865.

Liu, L., Zhang, H., Xie, J., Zhao, Q., 2021. Dynamic evacuation planning on cruise ships based on an improved ant colony system (IACS). J. Mar. Sci. Eng. 9 (2), 220.

Mahdevari, S., Shahriar, K., Esfahanipour, A., 2014. Human health and safety risks management in underground coal mines using fuzzy TOPSIS. Sci. Total Environ. 488–489 (1), 85–99.

Neumann, M., 1984. A ford-fulkerson type theorem concerning vector-valued flows in infinite networks. Czechoslovak Mathematical Journal 34 (1), 156–162.

Nevill, A.M., Holder, R.L., 1995. Scaling, normalizing, and per ratio standards: an allometric modeling approach. J. Appl. Physiol. 79 (3), 1027–1031.

Occupational Safety and Health Administration (OSHA), 2012. Carbon Monoxide Poisoning. Report, URL: https://www.osha.gov/sites/default/files/publications/carbonmonoxide-factsheet.pdf.

Onifade, M., 2021. Towards an emergency preparedness for self-rescue from underground coal mines. Process Saf. Environ. Prot. 149, 946–957.

Ray, S.K., Singh, R.P., 2007. Recent developments and practices to control fire in underground coal mines. Fire Technol. 43 (4), 285–300.

Roy, S., Mishra, D.P., Bhattacharjee, R.M., Agrawal, H., 2022. Heat stress in underground mines and its control measures: A systematic literature review and retrospective analysis. Min., Metall. Explor. 39, 357–383.

Ryan, L., Watkinson, M., 2017. Underground coal mine gas monitoring emergency preparation. In: Proceedings of the 2017 Coal Operators' Conference. pp. 326–331.

Sasmito, A.P., Birgersson, E., Ly, H.C., Mujumdar, A.S., 2013. Some approaches to improve ventilation system in underground coal mines environment - A computational fluid dynamic study. Tunn. Undergr. Space Technol. 34, 82–95.

SRK Consulting (Global) Lmt., 2023. Minefire mass flow ventilation network simulator. URL: https://www.srk.com/en/products/minefire-mass-flow-ventilation-network-simulator.

Szurgacz, D., Sobik, L., Brodny, J., 2019. Inter gases as one of the ways to reduce the risk of endogenous fires in hard coal mines. Multidiscip. Aspects Prod. Eng. 2 (1), 183–190.

Thunderhead Engineering, 2023. PyroSim. URL: https://www.thunderheadeng.com/pyrosim.

United Nations Environment Programme and World Health Organization, 1972. Carbon monoxide executive summary. pp. 5–16.

US Department of Labor and MSHA, 2007. Carbon Monoxide and Mining - Health Hazard Information Card HH-28. Report.

US Department of Labor and MSHA and National Mine Health and Safety Academy, 2012. Heat Stress in Mining. Report, URL: https://www.msha.gov/safety-and-health/safety-and-health-materials/heat-stress.

Vuma Software, 2023. VUMA-Network interactive network simulation software. URL: https://www.vuma3d.com/vuma-network/.

World Health Organization, 1979. Carbon monoxide. World Health Organization.

Yang, B., Yao, H., Wang, F., 2022a. A review of ventilation and environmental control of underground spaces. Energies 15 (2).

Yang, X., Zhang, R., Li, Y., Pan, F., 2022b. Passenger evacuation path planning in subway station under multiple fires based on multiobjective robust optimization. IEEE Trans. Intell. Transp. Syst. 23 (11), 21915–21931.

Yu, X., Chen, W.-N., Hu, X.-M., Gu, T., Yuan, H., Zhou, Y., Zhang, J., 2019. Path planning in multiple-AUV systems for difficult target traveling missions: a hybrid metaheuristic approach. IEEE Trans. Cogn. Dev. Syst. 12 (3), 561–574.

Zhou, L., Schall, J., 2020. MFIRE 4.0 enhances fire modeling capabilities. URL: https://www.cdc.gov/niosh/mining/works/coversheet2169.html.